Journal of Materials Chemistry A

ROYAL SOCIETY OF CHEMISTRY

REVIEW

View Article Online
View Journal | View Issue

Cite this: J. Mater. Chem. A, 2021, 9, 6732

Insights into iodoplumbate complex evolution of precursor solutions for perovskite solar cells: from aging to degradation

Bo Li,[a] Qilin Dai, *[b] Sining Yun*[c] and Jianjun Tian *[a]

The power conversion efficiency (PCE) of solution-processed perovskite solar cells (PSCs) is significantly influenced by the characteristics of the perovskite precursor solutions. Iodoplumbate complexes such as PbI_2, PbI_3^-, and PbI_4^{2-} present in perovskite precursor solution in equilibria dictate the quality of perovskite films and the corresponding optoelectrical performance of PSCs. Meanwhile, the solvent and additive molecules compete with I^- to coordinate with Pb^{2+} and shift the chemical equilibria based on their coordination capabilities. The proportion and species of iodoplumbate complexes have a time-dependent influence on the subsequent perovskite crystallization and the quality of perovskite films. This review presents the impact of the evolution of the characteristics of a perovskite precursor solution driven by the components of the precursor solution, aging, degradation, and humidity on the physical properties of perovskite films and the photovoltaic performance of PSCs. A brief outlook on further improving the reproducibility window for PSCs fabricated by the solution process is provided based on the current research progress in terms of perovskite precursor evolution in PSCs.

Received 13th December 2020
Accepted 11th February 2021

DOI: 10.1039/d0ta12094d

rsc.li/materials-a

1. Introduction

Since the discovery of methylammonium lead halides ($MAPbX_3$, $X = Cl^-$, Br^-, and I^-) in 1978, the excellent optical and electronic properties of organic–inorganic hybrid metal halide perovskite materials have been intensively investigated for several decades.[1–4] Polycrystalline $MAPbI_3$ exhibits a direct bandgap (~1.55 eV),[5] high optical absorption coefficient (1.5×10^4 cm^{-1} at 550 nm),[6] low Urbach energy (~15 meV),[7] small exciton binding energy (2–75 meV),[8,9] high charge carrier mobility (10–24 cm^2 V^{-1} S^{-1}),[9,10] long carrier diffusion length (up to 1 μm),[11] low trap density (10^{15} to 10^{16} cm^3),[9,12,13] and low crystallization activation energy (97.3 kJ mol^{-1}),[14] making it a promising semiconductor material for light-energy conversion.[15] The pioneering work on hybrid lead halide perovskite sensitized solar cells was reported by Miyasaka and co-workers

[a]Institute of Advanced Materials and Technology, University of Science and Technology Beijing, 100083, China. E-mail: tianjianjun@mater.ustb.edu.cn

[b]Department of Chemistry, Physics, and Atmospheric Sciences, Jackson State University, Jackson, MS, 39217, USA

[c]Functional Materials Laboratory (FML), School of Materials Science and Engineering, Xi'an University of Architecture and Technology, Xi'an, Shaanxi, 710055, China

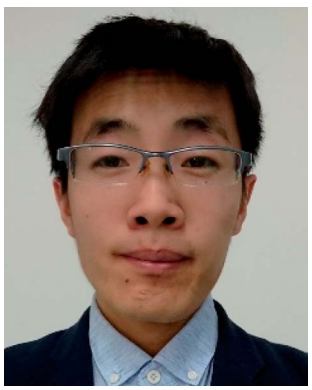

Bo Li earned his PhD degree from the University of Science and Technology Beijing in 2019 under the supervision of Prof. Jianjun Tian. His study was focused on the fabrication of highly efficient perovskite solar cells in the Laboratory of Optoelectronic Materials and Devices. From 2019 to 2020, he worked as a postdoctoral researcher at Jackson State University USA. His research focuses on perovskite precursor solution chemistry.

Dr Qilin Dai is an assistant professor of physics at Jackson State University, USA. He earned his PhD degree in Condensed Matter Physics from the Chinese Academy of Sciences in 2009, and then served as a post-doctoral research associate in the USA at Florida State University and the University of Wyoming. His research interests include (1) perovskite solar cells with high stability and high efficiency and (2) nanosized metal oxide synthesis for energy storage devices.

in 2009;[16] the devices showed poor stability due to the rapid dissolution of perovskite nanocrystalline particles in the liquid electrolyte that was commonly used in dye-sensitized solar cells.[17] Interest in photovoltaics has increased sharply since the emergence of solid-state perovskite solar cells (PSCs) in 2012.[6,18–24] So far, highly efficient PSCs have achieved a certified power conversion efficiency (PCE) of 25.5%.[25] However, large PCE differences were reported among worldwide research groups, even adopting the same device architecture and solution process.[26–29] There is an increasing consensus that the characteristics of the perovskite precursor solution are predominately responsible for the PCE differences.

Recently, perovskite precursor solution chemistry has received intensive attention concerning its relationship with the physical properties of perovskite films.[30–33] Perovskite precursor solutions are known as colloidal dispersions on the mesoscale. The inorganic component PbI_2 undergoes complexation with the organic component CH_3NH_3I (MAI) to form several iodoplumbate complexes, which serve as precursors in the solution. Yan and co-workers first revealed that MAI could coordinate with the trigonal PbI_2 colloid to form tetragonal iodoplumbate coordination complexes, or even corner-sharing and individual PbI_6^{4-} octahedral units with a maximum coordination number, depending on the content of MAI. It indicates that the colloidal framework of iodoplumbate coordination complexes could be structurally tuned by the stoichiometric ratio of PbI_2 : MAI, which will determine the final perovskite morphology and crystallinity.[30] Besides, the solvent–solute and additive-solute interactions also affect the species of iodoplumbate complexes in the precursor solutions and play a critical role in the subsequent perovskite crystallization,[34–36] since the solvent and additive molecules are prone to compete with I^- for coordination sites around Pb^{2+} according to their coordination capabilities, and thus control the perovskite formation.[37] For example, the incorporation of 10 mM I_3^- into the perovskite precursor solution was reported to produce smaller high-valent clusters, which were closely related to the enhanced crystallinity, homogeneous chemical composition, and less defect concentration of the resulting perovskite films, as well as the improved efficiency of PSCs.[29] Moreover, the status of perovskite precursor solutions changes during storage. High-quality perovskite films can only be achieved within the optimal precursor solution aging time because the perovskite precursor solutions suffer from degeneration during long-term aging.[38–40] It is noteworthy that many different variations of solution-based deposition techniques of perovskite films have been investigated over the years, such as spin coating,[41] spray coating,[42] slot-die coating,[43] doctor-blade coating,[44,45] and inkjet printing;[46,47] the optimal precursor solution concentration, stoichiometry, and composition may vary to meet desired crystallization kinetics in each case. However, for solution-processed PSCs, the characteristics of the perovskite precursor solution have been demonstrated to constantly evolve until reaching chemical equilibria.[38,39,48] Although several review articles have described the fundamental understanding of the nucleation and growth mechanism and microstructural evolution of perovskite from the precursor solution to a crystalline solid phase,[32,33,49] only a few reports focused on the time-dependent influence of the characteristics of the perovskite precursor solution on the subsequent perovskite film quality and the corresponding device performance.

In this review, we explore the impact of the characteristics of perovskite precursors on the photovoltaic performance of PSCs. A fundamental understanding of the intrinsic relationships between the perovskite precursor solution chemistry and the physical properties of the perovskite films is presented. Then we summarize the evolution of iodoplumbate coordination complexes in perovskite precursor solutions driven by aging,

Sining Yun is a Professor in the School of Materials & Mineral Resources, Xi'an University of Architecture and Technology, China. He obtained his PhD degree from Xi'an Jiaotong University in 2007 and was a postdoctoral fellow at Yonsei University (Korea). He is a visiting professor at the State Key Laboratory of Fine Chemicals (China), University of Reading (UK), and Prof. Michael Grätzel and Prof. Anders Hagfeldt's laboratory at EPFL (Switzerland). He is currently a Research Director and Group Leader of the Functional Materials Laboratory and the Key Laboratory of Nanomaterials and Nanotechnology of Shaanxi Province (China). His research focuses on solar energy and biomass energy. Details can be found at: http://xy.xauat.edu.cn/gnclyjs/listyjsgk.asp?id=262&bh=2080.

Jianjun Tian is presently a professor at the Institute for Advanced Materials and Technology, University of Science and Technology Beijing. His current research is focused on the development of colloidal quantum dots and novel perovskite materials for the optoelectronic applications including the next generation solar cells, light-emitting diodes, and photodetectors.

degradation, and humidity with the consideration of their influence on the perovskite film quality. Finally, we provide a brief outlook on further improving the reproducibility window for PSCs fabricated by the solution process.

2. Perovskite precursor solution chemistry

2.1 Evolution of iodoplumbate complexes

The studies on the coordination chemistry of lead(II) have been well established over the past decade. The 6 s^2 electron pair of lead(II) is stereochemically active and plays a role in the complexation with halide ions and solvents.[50,51] In 1940, Lanford and co-workers found that the solubility of lead iodide (PbI_2) in the solution increased in the presence of iodide ions, which could be explained by the formation of the complexes of PbI_3^- and PbI_4^{2-}.[52] Similar complexation between PbI_2 and halide ions occurs in perovskite precursor solutions. Fig. 1(a) shows absorption spectra of a PbI_2 solution with gradual increase of the MAI concentration; the appearance of two new concentration-dependent absorption bands with maxima at 370 and 425 nm confirms the presence of two separate complexes of PbI_3^- and PbI_4^{2-}, and the equilibria between PbI_2, PbI_3^-, and PbI_4^{2-} can be described as eqn (1) and (2)

$$PbI_2 + I^- \overset{K_1}{\longleftrightarrow} PbI_3^- \quad (1)$$

$$PbI_3^- + I^- \overset{K_2}{\longleftrightarrow} PbI_4^{2-} \quad (2)$$

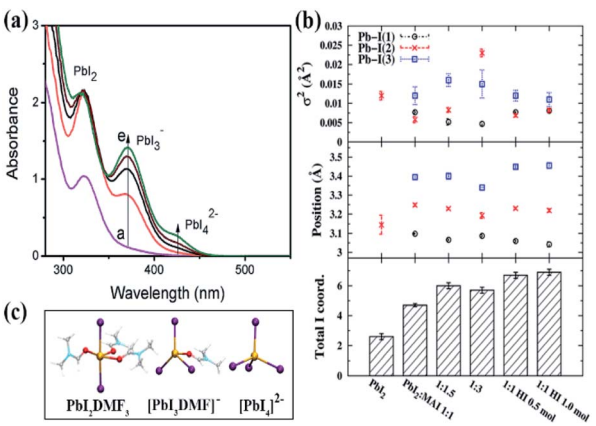

Fig. 1 (a) Absorption spectra of 250 μM PbI_2 solution in dimethylformamide with increasing concentration of MAI from 6 mM to 24 mM. Reprinted from ref. 53 with permission from the Royal Society of Chemistry. (b) Real-space extended X-ray absorption fine structure (EXAFS) fit parameters. The top panel plots the correlated Debye–Waller factor (σ^2), the middle panel the Pb–I components' positions from the absorbing Pb atom, and the bottom panel the total iodide coordination number of the Pb atoms in solution. Note that the disorder increases as the value of σ^2 increases and the Pb atoms in both PbI_2 and $MAPbI_3$ exhibit octahedral iodide coordination (PbI_6). Reprinted from ref. 54 with permission from the American Chemical Society. (c) Optimized geometries for selected $[PbI_mX_n]^{2-m}$ iodoplumbate complexes in DMF. Reprinted from ref. 55 with permission from the American Chemical Society.

the estimated complexation constants of K_1 and K_2 for two equilibria are 54 and 6 M^{-1} in *N*,*N*-dimethylformamide (DMF).[53] To further investigate the exact structure of iodoplumbate complexes, Toney and co-workers investigated the local structure of the Pb^{2+} ions in precursor solutions as a function of the precursor molar ratio using X-ray absorption spectroscopy (Fig. 1(b)).[54] A single Pb–I component with a distance of ~3.1 Å is well fitted for the PbI_2 only solution. In contrast, three Pb–I components with distinct distances of ~3.1, ~3.2–3.25, and ~3.4 Å are observed from the solutions containing PbI_2 and MAI. Considering the lack of comparable Pb–I bond lengths in PbI_2 or $MAPbI_3$ to match the fitted distances, it is reasonable to speculate that the mismatched Pb–I components originate from the extended octahedral Pb–I fragments in the iodoplumbate complexes. Despite the 10–15% systemic error for the coordination numbers from the fitted data, the Pb ions' total iodide coordination generally increases with increasing I^- concentration, consisting of the concentration-dependent absorption bands mentioned above. It is worth noting that the total iodide coordination number is ~5 in the case of PbI_2 : MAI = 1 : 1, indicating that Pb^{2+} is not fully coordinated with six I^- ions in the standard perovskite precursor solution. Excess MAI or other iodide sources are needed to achieve the full coordination of Pb^{2+}. The results are consistent with the fact that solvent molecules can compete with I^- for the coordination sites of Pb^{2+}, depending on their coordinating capabilities, which inhibit the formation of high order iodoplumbate complexes. Based on density functional theory (DFT) calculations, the computational absorption spectra based on the optimized geometries of iodoplumbate complexes, including PbI_2DMF_3, $[PbI_3DMF]^-$, and PbI_4^{2-} (Fig. 1(c)), show characteristic absorption at 311 nm, 375 nm, and 416 nm, respectively, which closely match the experimental results as shown in Fig. 1(a).[55] The result further confirms the presence of solvated iodoplumbate complexes in the precursor solution.

To establish the atomic origin and the evolution of these iodoplumbate complexes, Ahlawat and co-workers employed well-tempered metadynamics simulations to reveal the time evolution of iodoplumbate complexes in a perovskite precursor solution with γ-butyrolactone (GBL) as the solvent.[56] In a well-equilibrated solution where the MA^+, Pb^{2+}, and I^- ions are initially homogeneously distributed in GBL, the iodoplumbate complexes of PbI_2, PbI_3^-, and PbI_4^{2-} emerge spontaneously. The increased coordination of Pb^{2+} with I^- ions contributes to the formation of face- or edge-sharing PbI_6^{4-} octahedral clusters after ~130–140 ns (Fig. 2). Then MA^+ ions surround these clusters to balance the negative charge. The edge-sharing PbI_6^{4-} octahedra start to transform into a PbI_2-like structure by sharing at least three edges with neighboring PbI_6^{4-} octahedra after 150 ns. As a result, the open structure enables the diffusion of MA^+ ions in these spaces and eventually transform into PbI_4^{2-} tetrahedra. Around 180 ns, this tetrahedral structure rearranges into corner-sharing PbI_6^{4-} octahedra with the MA^+ ions in the center. These simulation results are in general agreement with the experimental observation of PbI_6^{4-} octahedral cage nanoparticles during perovskite crystallization.[57] Finally, the amorphous clusters partially transform into the

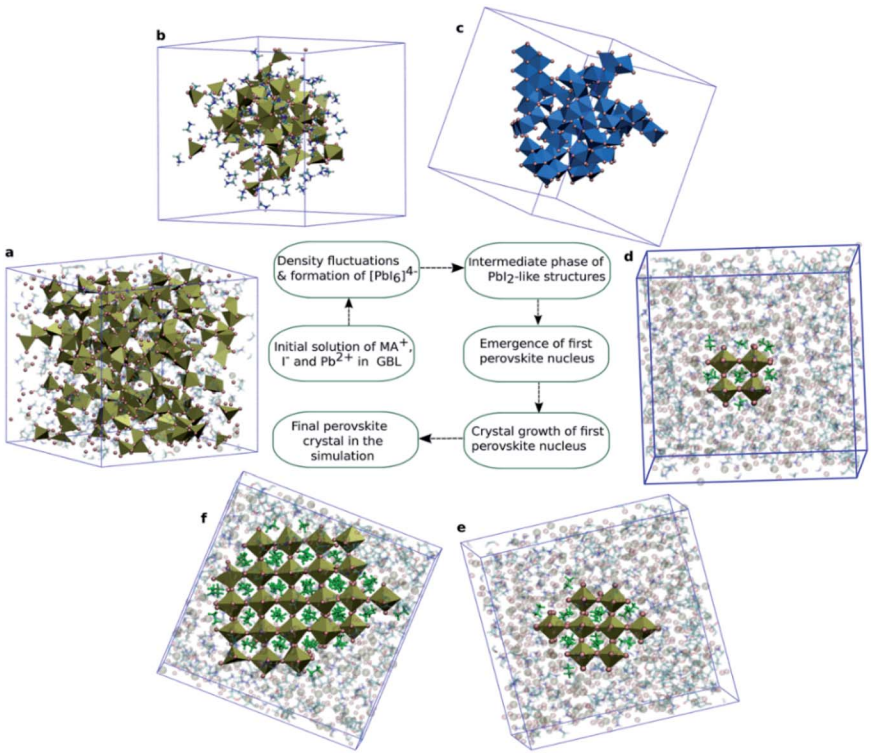

Fig. 2 (a) Initial solution of MA^+, I^-, and Pb^{2+} in GBL. MA^+ and GBL are shown semitransparent to visualize the random distribution of Pb^{2+} and I^- in solution. (b) Initial cluster formation of Pb^{2+} and I^- surrounded by MA^+ ions. (c) Edge-sharing $[PbI_6]^{4-}$ octahedra. (d) First perovskite nucleus observed in the solution. (e) Growth of the initial nucleus. (f) The largest perovskite crystal in the simulations. Reprinted from ref. 56 with permission from the American Chemical Society.

perovskite structure accompanied by the growth of perovskite crystals by the arrangement of ions around the initial nucleus. Based on the discussion above, we can now conclude that the perovskite precursor solution consists of solvated iodoplumbate complexes in a polar organic solvent or mixed solvents, and the species of iodoplumbate complexes evolve with the stoichiometric ratio or concentration of precursors until reaching equilibria.

2.2 Relationships with the physical properties of perovskite films

With the in-depth understanding of the perovskite precursor solution chemistry, there is an increasing consensus that the subtle changes of precursor solution parameters, including the precursor solution concentration, stoichiometry, temperature, and aging time, can result in a substantial variation in the physical properties of perovskite films. Fig. 3 summarizes the variability that often occurs in the physical properties of perovskite films induced by the characteristics of precursor solutions, such as the phase transition, morphology, crystallinity, component, and defect density.

2.2.1 Phase transition. Perovskite crystallization involves multistep phase transition, since the solvent and additive molecules are known to compete with I^- ions for the coordination sites of Pb^{2+} ions based on their coordination capabilities, and the solvated iodoplumbate complexes involved in both precursor solutions and precursor films are commonly observed.[58–64] For example, the presence of solvated iodoplumbate complexes in perovskite precursor solutions, including $PbIS_5^+$, PbI_2S_4, $PbI_3S_3^-$, $PbI_4S_2^{2-}$, and $PbI_5S_2^{3-}$ (S = solvent), has been confirmed. The lower the coordination capability of solvents, the higher the number of coordinated I^-

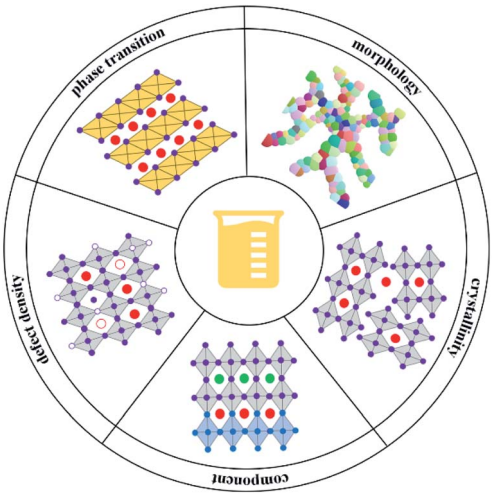

Fig. 3 Schematic representation of the influence of the perovskite precursor solution on the phase transition, morphology, crystallinity, component, and defect density of perovskite films.

ions in the iodoplumbate complexes.[65] In early studies on perovskite crystallization, the interaction of DMF with MAI and PbI_2 was studied, and it was reported that the addition of MAI into the precursor solution weakened the interaction between PbI_2 and DMF by intercalation into the PbI_2 framework.[66] $MAPbI_3$ dominant phases with a small amount of $(MA)_2(DMF)_2Pb_2I_6$ intermediate phase obtained from the perovskite precursor solution in DMF were widely reported.[35,67,68] In contrast, as shown in Fig. 4(a), in the case of stoichiometric precursors in a dimethylpropyleneurea (DMPU) solution, no discernible iodoplumbate characteristic absorbance can be observed because DMPU has a stronger affinity to Pb^{2+} compared to DMF and I^-.[37] As a result, a much more stable solvated intermediate phase is formed during perovskite formation instead of a crystalline perovskite structure. Therefore, the solvent–solute and additive–solute coordination play critical roles in perovskite crystallization. Iodoplumbate complexes containing a higher content of coordinated I^- in the precursor solutions with weak coordination solvents or additives are requisite for the formation of a perovskite structure.[65] In comparison, strong coordination solvents or additives reduce the number of coordinated I^- ions in iodoplumbate complexes and will suppress the perovskite formation.

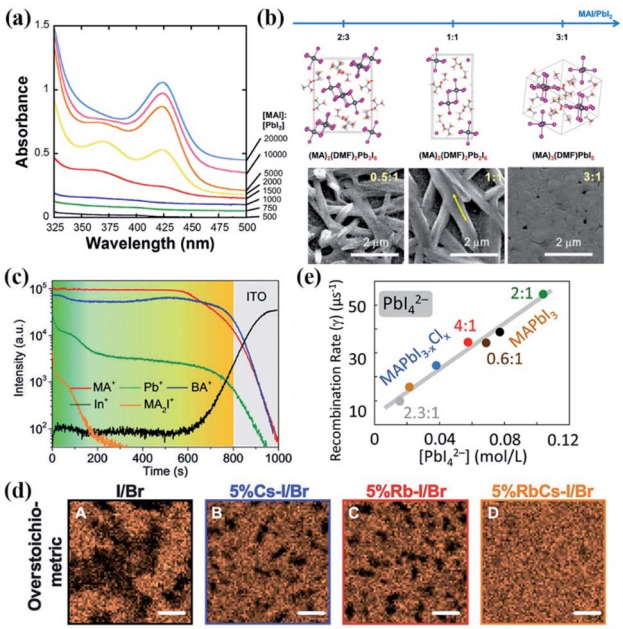

Fig. 4 (a) Absorbance of 0.05 mM PbI_2 with increasing [MAI] in DMPU. Spectral features corresponding to PbI_3^- at 370 nm and PbI_4^{2-} at 425 nm are evident only at [MAI] : [PbI_2] equal to or exceeding 1500. For [MAI] : [PbI_2] less than 1500, the absorbances of PbI_3^- and PbI_4^{2-} are negligible. Reprinted from ref. 37 with permission from the American Chemical Society. (b) Crystal structure motifs of three intermediate phases: PbI_2-rich $(MA)_2(DMF)_2Pb_3I_8$, stoichiometric $(MA)_2(DMF)_2Pb_2I_6$, and MAI-rich $(MA)_3(DMF)PbI_5$ and the corresponding SEM micrographs of calcined thin films with CH_3NH_3I coordination engineering. Reprinted from ref. 68 with permission from the American Chemical Society. (c) ToF-SIMS patterns of $BA_2MA_3Pb_4I_{13}$ films prepared at 70 °C. Reprinted from ref. 90 with permission from Wiley. (d) X-ray fluorescence mapping indicates the heterogeneous distribution of Br as a function of alkali metal stoichiometric composition of the perovskite films. Scale bars, 2 mm. Reprinted from ref. 91 with permission from the American Association for the Advancement of Science. (e) Correlation of iodoplumbate and iodide species present in precursor solutions *versus* charge recombination rates measured in the perovskite films deposited from the corresponding solutions. Reprinted from ref. 96 with permission from the American Chemical Society.

Solvent engineering and additive strategies have been successfully developed to modulate the precursor coordination and achieve controlled perovskite nucleation and crystal growth.[64,69–71] To date, dimethyl sulfoxide (DMSO) as the dominant coordinating molecule is used to retard the fast interaction between MAI and PbI_2, leading to the formation of a PbI_2·MAI·DMSO intermediate phase.[58,59,72] By controlling the mole ratio of DMSO : PbI_2 to 10 : 1 in perovskite precursor solutions, a pure $(MA)_2Pb_3I_8(DMSO)_2$ intermediate phase was obtained.[73] This induced the up-growth feature of perovskite films without horizontal grain boundaries. However, this retarding perovskite crystallization strategy often needs the extra steps of anti-solvent extraction,[58] gas-quenching,[74] or vacuum-assisted drying[19] to rapidly remove the solvents from wet films, which increases the complexity of the film deposition process and is detrimental to device reproducibility. By the integration of solvent engineering and additive strategies, a spontaneously supersaturated nucleation strategy was devised to fabricate high-quality perovskite films without any additional steps.[75] The incorporation of strong coordination additives into perovskite precursor solutions with a weak coordination solvent of 2-methoxyethanol (2-ME) could suppress the interaction of Pb^{2+} with I^- and solvent, leading to the precipitation of PbI_2-like coordination complexes in solutions. Volatile methylamine ethanol was further employed as a second solvent to dissolve these PbI_2-like coordination complexes. As a result, the rapid dissolution-precipitation behavior of the precursor films could be triggered by the volatilization of MA ethanol, thereby achieving perovskite films with a uniform distribution of small-sized intermediate phase grains. During annealing, the growth of densely packed nanometer-sized intermediate phase grains results in mirror-like and compact large-area perovskite films (10 cm × 10 cm) with enhanced crystallinity. Finally, an average PCE of 19.4% was achieved for small area PSCs (0.1 cm^2) due to the good reproducibility of high-quality perovskite films.

2.2.2 Morphology. As mentioned above, Pb^{2+} is not fully coordinated with six I^- ions in the stoichiometric perovskite precursor solution, and the PbI_2·DMF related crystals coordinated with some MAI tend to precipitate from the supersaturated precursors before perovskite crystals during an uncontrolled perovskite solidification,[76] leading to needle-like crystals as widely reported in the early literature.[41,74,77] In our previous work, we found that the solutes in the perovskite precursor solution divided into white MAI upper powder and yellow PbI_2 bottom powder after anti-solvent extraction, indicating that there is a weak interaction between MAI and PbI_2.[78] The two components can be bridge linked by 2-aminoethanethiol (2-AET) and form a stable coordination complex MAI·2-AET·PbI_2 in the perovskite precursor solution, which avoids the first precipitation of PbI_2·DMF related crystals and facilitates the formation of compact $MAPbI_3$ films with

polygonal grains. It implies that the origin of the needle-like morphology is closely related to the species of iodoplumbate complexes in perovskite precursor solutions. The type of initial iodoplumbate complex formed in the precursor solution can be determined by the stoichiometric ratio of precursors.[53] In a I^- ion deficient environment, more Pb^{2+} ions share the same I^- in the structure and increase the proportion of lower-order iodoplumbate complexes. As a result, the intermediate phase consisting of an edge- or face-sharing Pb–I octahedra forms in the precursor film (Fig. 4(b)). Such ribbon-like structure shows high anisotropy of the surface energy for growing crystals, which should be responsible for the needle-like morphology. In contrast, the isolated corner-sharing Pb–I octahedra with a higher proportion of I^- ions dominate the intermediate phase in I^- ion-rich precursor films, and the low anisotropy of the surface energy of the structure will achieve equiaxed growth of perovskite grains and facilitate the formation of a more uniform morphology.[30,68]

In addition, we found that the introduction of methylammonium chloride (MACl) into the perovskite precursor solution significantly increased the colloidal cluster size through coordination interaction.[13] The large colloidal clusters were orderly arranged on the substrate and grown to form large grains with an average size of 3 μm after annealing. Similar results were observed for the precursor solution with the addition of methylammonium thiocyanate (MASCN).[79] Han and co-workers demonstrated that the perovskite grain size in the final films strongly depends on the sizes of iodoplumbate complexes in precursor solutions. The grain sizes of the corresponding perovskite films increased from 100 nm to 2 μm for 0–50% MASCN additive levels.

2.2.3 Composition. Excellent progress has been made on the incorporation of monovalent cations into perovskite precursor solutions to achieve an enhanced quality of the perovskite films and improved device performance. In particular, the incorporation of formamidinium (FA) and alkali metal cations, including Cs, Rb, and K, into the precursor solutions has led to further improvement of the efficiency of PSCs and enhanced stability at elevated temperatures.[80–85] Besides, long-chain ammonium cations are introduced to transform the perovskite structure into a more stable two-dimensional (2D) Ruddlesden–Popper perovskite against humidity.[86–88] However, the mixed compositions in perovskite films suffer from compositional inhomogeneity and phase-segregation. For example, the fluorescence signals originating from the perovskite side and the backside showed significantly different peak positions for most 2D Ruddlesden–Popper perovskite films due to the composition difference along the cross-sectional direction.[86,89] Recently, based on Fick's second law, Liu and co-workers investigated the cation diffusion process in a precursor film containing mixed organic cations using the diffusion model.[90] They found the flux drop of MA^+ is more significant than that of the butylamine cation (BA^+) across the same regions of the film, so the distribution of MA^+ decreases progressively from the surface to the bottom and leads to a composition change, as evidenced by time-of-flight secondary ion mass spectrometry (TOF-SIMS) as shown in Fig. 4(c). Based on the diffusion model, employing solvents with low boiling points enables a much shorter gel duration time for significantly suppressing the cation diffusion and achieving homogeneous and phase segregation free perovskite films in mixed cation systems.

Apart from the A site cation-initiated phase segregation, the halide anions are reported to form some anion-poor/rich phases. In our recent work, the Cl-rich phase-initiated precipitation behavior of the precursor solution was observed in the perovskite precursor solution with a weak coordination solvent of 2-methoxyenthanol (2-ME), leading to the formation of a Cl-rich intermediate phase in the precursor films.[75] With the help of synchrotron-based nano-X-ray fluorescence, Correa-Baena and co-workers reported that although enhanced efficiency can be achieved in the case of perovskite films prepared from over-stoichiometric PbX_2 and AX (X = halide anion) precursor solutions, large clusters of lower Br content with sizes of 6–8 μm on the perovskite films are observed, while the area fraction reduces to 32%, 29%, and only ~6% upon the addition of RbI, CsI, and a mixture of RbI and CsI (Fig. 4(d)), respectively.[91] However, the incorporation of alkali metals with a higher concentration produces optoelectronically inactive, current blocking, and possibly recombination-active clusters on perovskite films, which is detrimental to the PSC performance. It is noteworthy that the segregation of highly concentrated Rb clusters was also observed on the perovskite films obtained from the precursor solution even with added 1% Rb. Therefore, careful attention to the composition difference in the mixed cation or anion perovskite films is required and will benefit the development of highly reproducible optoelectronic devices.

2.2.4 Defect density. Perovskite exhibits a high tolerance for intrinsic defects, the common point defects in perovskite films are shallow states in the forbidden band, while the iodine interstitials, or iodine vacancies are known as as deep-level defects.[92–95] The origin of such defects in the bulk of perovskite is also considered to be directly correlated with the perovskite precursor solution chemistry. Stewart and co-workers established a correlation between the concentration of iodoplumbate complexes in precursor solutions and the recombination rate of the corresponding perovskite films (Fig. 4(e)).[96] They found that only the concentration of PbI_4^{2-} is uniquely correlated with the density of charge recombination centers. In parallel to the study for revealing the relationship between precursor solutions and the defect of perovskite films, Kim and co-workers found that in an I^- rich perovskite precursor solution, the equilibria of iodoplumbate complexes shift toward higher-order iodoplumbate complexes and result in high-valent clusters with a reduced colloidal particle radius.[29] These results are in good agreement with the discussion in Section 2.1. Compared to the control sample, the perovskite films derived from the high-valent cluster containing precursor solution show enhanced crystal orientation, higher surface homogeneity, a longer non-radiative charge carrier lifetime, and a lower defect density of 3.77×10^{-15} cm^3, yielding a significant improvement of PCE from 17.51% to 20.6%. Therefore, the precise control of the proportion and species of iodoplumbate complexes present in

perovskite precursor solutions plays a vital role in the fabrication of highly efficient PSCs.

3. Perovskite precursor solution aging effect

As discussed above, the perovskite precursor solution is composed of several iodoplumbate complexes in a polar aprotic organic solvent or mixed solvents, in which I^- ions and solvent molecules are prone to coordinate with the Pb^{2+} ions. The incorporation of additives is expected to shift the equilibria position depending on their coordination capabilities, thus changing the distribution proportion and species of iodoplumbate complexes until reaching new chemical equilibria. Therefore, the evolution of iodoplumbate complexes during precursor solution aging will have a time-dependent influence on the subsequent perovskite crystallization and the quality of perovskite films.

3.1 Perovskite precursor aging

It was reported that single precursor chemicals, such as FAI, MABr, PbI_2, and $PbBr_2$, could not be fully dissolved in a mixture of DMF/DMSO solvents within 2 h at room temperature.[97] In this regard, the perovskite precursor solution needs a certain aging treatment to form a homogeneous solution, and this will have a time-dependent impact on the perovskite film quality as well. For example, a three-week-aged $CsPbIBr_2$ precursor solution was reported to allow the fabrication of pure-phase and full-coverage $CsPbIBr_2$ films with a lower formation temperature, and the PCE increased to 6.55% compared to only 3.36% for the PSCs derived from the nonaged precursor solution.[98]

In a recent study, Su and co-workers investigated the aging effect of perovskite precursor solutions stored at different temperatures on the photovoltaic performance of PSCs.[38] As shown in Fig. 5(a–c), for the precursor solution aged at 4 °C, the average PCE increased from 16.48% to 17.29% after 24 h aging treatment, and then it decreased to 15.73% upon further aging for 96 h. The aging effect was increased in the case of the precursor solution aged at room temperature. 2–4 h aging yielded a higher PCE of ~17.5% compared to 16.48% for the PSCs obtained from the fresh solution. A more increased aging effect was achieved upon aging the precursor solutions at an elevated temperature of 65 °C. The highest PCE of ~17.1% was obtained from the solution aged for only 1.5 or 2 h. As expected, the optimal aging time is shortened as the aging temperature increases. Fig. 5(d) shows the UV-vis absorption spectra of the precursor solution at different aging times. The intensity of the distinct absorbance peak of $PbI_2[S]_4$ at 292 nm increased after aging for 1.5 h, and then it decreased for a longer aging of 3 h, indicating that the species of iodoplumbate complexes evolve with the precursor solution aging time. Since strong coordination solvent molecules can cause insufficient coordination between Pb^{2+} and I^- ions as mentioned in Section 2.1.1, an excess PbI_2 or MAI was introduced as an iodide source to induce the formation of sufficient $PbI_2[S]_4$ in precursor solutions, and in turn compensate for the aging effect. This is confirmed by little dependence of the intensity on the aging time from the UV-vis absorption spectra shown in Fig. 5(e and f). So, the proportion of iodoplumbate complexes in the precursor solutions is sensitive to the temperature and precursor stoichiometry and will impact the corresponding perovskite film quality.[99,100] The optimal operating window for perovskite precursor solutions under different storage conditions should be carefully adjusted.

3.2 Additive induced aging

The incorporation of additives into perovskite precursor solution has been demonstrated to control the crystallization kinetics and improve the perovskite film quality.[36,58,101–103] It is recognized that the additive induced aging effect is a critical parameter to affect the nucleation and growth of perovskite. For example, as shown in Fig. 6(a–e), the average grain-like size of perovskite films and PCE of the corresponding PSCs were found

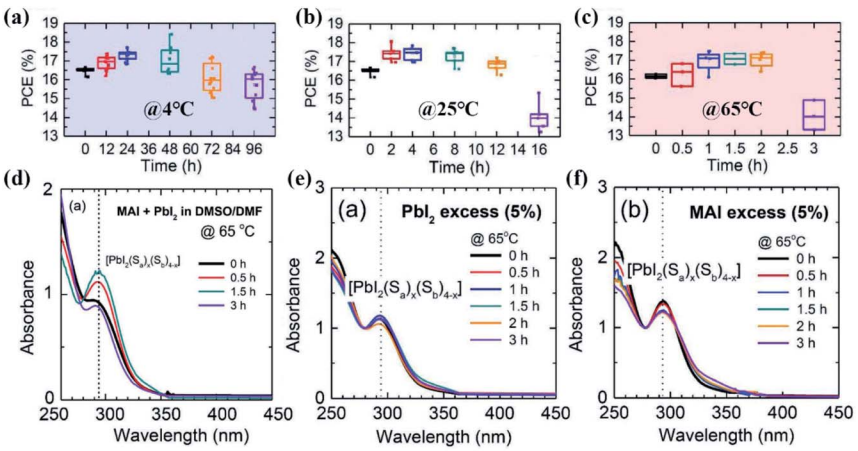

Fig. 5 PCE of mesoscopic normal structured perovskite solar cells employing $MAPbI_3$ films aged at (a) 4 °C, (b) room temperature (RT), and (c) 65 °C. The aging time was varied from 0 to 96 h at 4 °C, 16 h at RT, and 3 h at 65 °C. UV-vis absorption spectra of 10^{-4} M (MAI + PbI_2) precursor solution dissolved in DMSO/DMF without (d) and with excess PbI_2 (e) or excess MAI (f). Reprinted from ref. 38 with permission from Wiley.

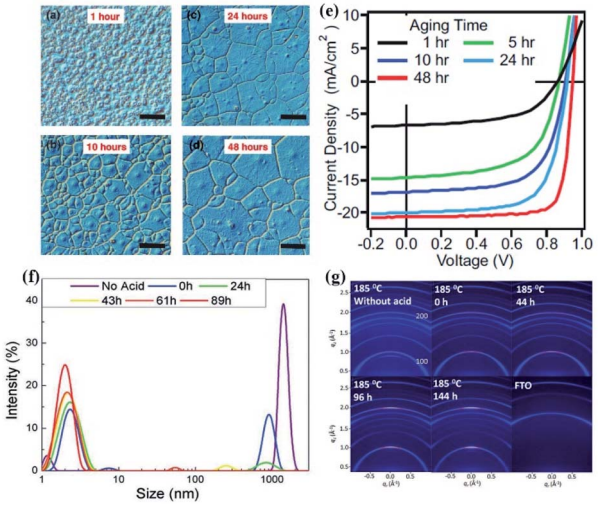

Fig. 6 Optical microscope images of perovskite thin films produced by hot casting. The precursors are aged for different time periods: (a) 1 h, (b) 10 h, (c) 24 h, and (d) 48 h. Scale bar: 50 μm. (e) Average grain-size with the error bar determined for 1–48 h aging time. Reprinted from ref. 39 with permission from Wiley. (f) Colloidal hydrodynamic size distribution *via* dynamic light scattering of various perovskite solutions. (g) A series of 2D X-ray diffraction patterns of the corresponding thin film after the annealing step. Reprinted from ref. 40 with permission from Wiley.

to increase with the precursor aging time for the precursor solution with the additive of methylammonium hydrochloride (MACl), accompanied by the increased colloidal size of iodoplumbate complexes in the precursor solution.[39] The result is consistent with the finding that the perovskite film grain size strongly depends on the precursor aggregate size in precursor solutions.[13,79] The authors speculated that the presence of nucleating iodoplumbate complexes and their size in the progressively aged precursor solution are directly correlated with the grain size in perovskite films. Based on the LaMer diagram, the nucleation of the iodoplumbate complexes induced by additives can be divided into three distinct processes: (1) prenucleation: a rapid increase in the concentration of free intermediates by dissolving the precursors and additive. (2) Burst nucleation: fast nucleation of iodoplumbate complex clusters coordinated with the additive. (3) Growth by diffusion: a decrease in the concentration of iodoplumbate complex clusters by forming larger crystallites. In parallel to the additive induced aging effect on the nucleation and growth of iodoplumbate complexes, the time-dependent reduction in the colloid size was reported for the precursor solution with a mixture of hydroiodic (HI) and hydrobromic (HBr) as additives (Fig. 6(f)).[40] The authors demonstrated that these iodoplumbate complexes would serve as nucleation centers in the formation of perovskite films. Therefore, the density of nucleation sites of the precursor film would be reduced with the solution aging time for the solutions with the additives of HI and HBr, so that the growth of perovskite crystals would likely be dominant during perovskite formation. As a result, larger polycrystalline grain domains with preferred orientation and higher mobility were obtained from the aged precursor solution (Fig. 6(g)).

As discussed above, the optimal precursor solution aging time ranges from several hours to a few tens of hours. It is reasonable to speculate that the coordination capabilities of I^- ions, solvent molecules, and additive molecules to Pb^{2+} may be comparable to each other, so it is difficult to overcome the energy barrier for the reconstruction of iodoplumbate complexes. Recently, a single perovskite crystal was reported as a solute to prepare the perovskite precursor solution, and high-quality perovskite films with reduced trap state density were obtained, as well as an impressive efficiency for PSCs.[104,105] We speculate that the single perovskite crystal in the precursor solution may reduce the energy barrier and suppress the structural defects in both gel precursor films and perovskite films. So, this strategy may further mitigate the precursor solution aging effect and improve the reproducibility of high-quality perovskite films.

4. Degradation of perovskite precursor solutions

So far, we have discussed the beneficial effect of precursor solution aging on the performance of PSCs. However, the perovskite precursor solution suffers from degeneration during long-term storage due to the chemical reactions between the precursor solution's components and the environmental condition induced degradation, which drastically decreases the photovoltaic efficiency of the corresponding PSCs.

4.1 Chemical reactions between components

Several studies focused on the chemical reactions between the solute and solvent occurring in perovskite precursor solutions. For example, proton transfer from MA^+ to DMSO has been demonstrated in the perovskite precursor solution containing the MAI component and DMSO, in which the MA^+ induces proton transfer to DMSO to form methylamine (CH_3NH_2), followed by methyl group transfer between CH_3NH_2 and residual MA^+, resulting in ammonium (NH_4^+) and dimethylammonium (DMA^+) (Fig. 7(a)).[106] Meanwhile, the transmethylation from DMSO to MA^+ leads to the formation of DMA^+ and methylsulfonic acid (CH_3SOH). Then CH_3SOH can react with DMSO quickly to form methylsulfinic acid (CH_3SOOH) and dimethylsulfide (CH_3SCH_3). Finally, the produced CH_3SOOH undergoes further reaction with DMSO to form methylsulfonic acid (CH_3SO_3H) and another equivalent of CH_3SCH_3. The deprotonation of MA^+ and the subsequent methyl group transfer represent the dominant pathway and introduces the cation impurities of NH_4^+ and DMA^+ into the perovskite precursor solutions.

Except for the solute–solvent reactions in precursor solutions, the MAI and FAI contents in a mixed organic cation perovskite precursor solution were found to reduce sharply along with the aging time.[107] In contrast, little changes occurred in the pure $MAPbI_3$ precursor solution. It implies that there are potential chemical reactions between the two organic cations. As shown in Fig. 7(b), Wang and co-workers proposed the possible reactions in a co-existing perovskite precursor solution

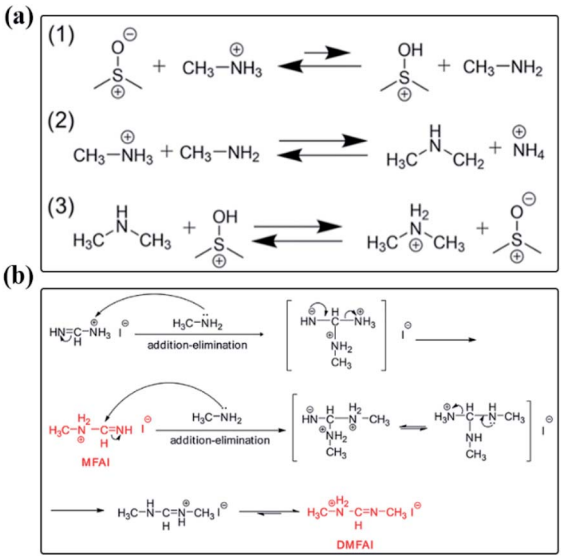

Fig. 7 Possible reaction mechanism in perovskite precursor solutions. (a) Formation of DMA^+ and NH_4^+ in DMSO. Reprinted from ref. 106 with permission from the American Chemical Society. (b) The addition–elimination reactions between MA and FAI in the perovskite precursor solution. Reprinted from ref. 107 with permission from Elsevier Inc.

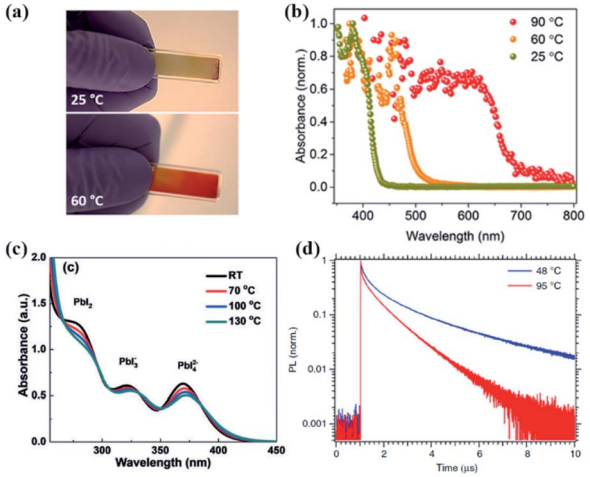

Fig. 8 Picture (a) and absorption spectra (b) of a TC prototype after annealing at different temperatures: 25 °C yellow, 60 °C orange, and 90 °C red. Reprinted from ref. 112 with permission from the American Chemical Society. (c) Absorption spectra of a precursor solution with a MAI : PbI_2 ratio of 1.7 at different temperatures. Reprinted from ref. 100 with permission from Wiley. (d) Photoluminescence decay of $MAPbI_3$ single crystals grown at 48 °C and 95 °C. Reprinted from ref. 108 with permission from the Nature Publishing group.

containing MAI and FAI. MAI is known to suffer from the deprotonation reaction and result in CH_3NH_2 in the solution. Due to the nucleophilicity of lone-pair electrons of the N atom in CH_3NH_2 and the active electrophilic imine bond in FAI, if the produced CH_3NH_2 could not volatilize, it would be constantly consumed by FAI through an addition–elimination reaction to form the condensation products of *N*-methyl FAI (MFAI). The formed MAFI also has an imine bond and is prone to induce a second addition–elimination reaction with CH_3NH_2 to produce *N*,*N*′-dimethyl FAI (DMFAI). Thus, the degradation products from the chemical reactions between the solute and solvent should be responsible for the low stability of perovskite precursor solutions.

4.2 Environmental factors

4.2.1 Temperature. Perovskite precursor solutions show inverse temperature solubility behavior; the solubility of the solute components in certain solvents decreases with increasing temperature. This phenomenon has been widely applied to obtain high-quality $MAPbX_3$ single crystals.[108–111] As shown in Fig. 8(a and b), in a mixed halide anion (Br^- and I^-) perovskite precursor solution with a solvent of γ-butyrolactone (GBL), a completely reversible chromatic variation ranging from yellow to dark red as the temperature increased from 25 to 90 °C is observed due to the various solubility of PbX_2 and MAX (X is a halide anion).[112] In fact, the chemical equilibria between iodoplumbate complexes in the GBL solution were found to shift to low order iodoplumbate complexes with increasing solution temperature ((Fig. 8(c))), along with the release of free ions from the iodoplumbates, which can explain the origin of saturation concentration for inverse temperature perovskite crystallization.[100] Nayak and co-workers investigated the effect of the solution temperature on the quality of single crystals.[108] They observed that the single crystals grown at lower temperature had less twining and an increased tilt between adjacent lead halide octahedra, yielding a lower nonradiative recombination site density in the bulk of the crystal (Fig. 8(d)). It suggests that the low order iodoplumbate complexes in the precursor solution with elevated temperature may cause defects in perovskite and reduce the perovskite film quality. Besides, as mentioned in Section 4.1.1, the chemical reactions between DMSO and MA^+ that occurred in the precursor solutions could be further promoted at higher temperature. This will produce more by-products DMA^+ and NH_4^+, which could not only incorporate into the perovskite structure as A-site impurities but also result in an increased density of states in the band gap of $MAPbI_3$.[106,113]

4.2.2 Light. Although light is known to be responsible for the observed accelerated degradation and ion migration of perovskite films and PSCs, as well as the crystal density during the perovskite film formation,[114–118] it can also impact the stability of perovskite precursor solutions. It is generally observed that the color of the perovskite precursor solution changes from transparent yellow to dark red with the aging time. In fact, due to the low redox potential, I^- ions are gradually oxidized to form molecular iodine (I_2) under UV radiation through a photochemical reaction as shown in eqn (3)

$$2I^- \overset{h\nu}{\longleftrightarrow} I_2 + 2e^- \quad (3)$$

which should be responsible for the color change in the precursor solution.[119,120] This process further leads to the formation of metallic lead (Pb^0) and iodine interstitials in perovskite films, which are commonly regarded as nonradiative

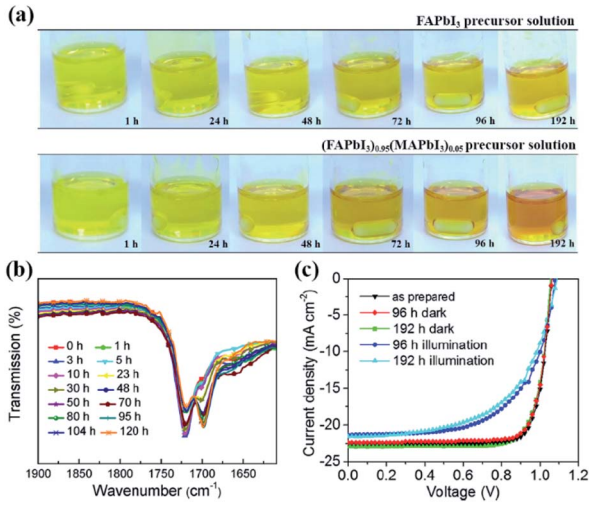

Fig. 9 (a) Perovskite precursor solution color change depending on time. $FAPbI_3$ black powder is dissolved in a mixed solvent of DMF/DMSO (top), a conventional perovskite precursor solution, wherein both $FAPbI_3$ and $MAPbBr_3$ powders are dissolved in the mixed solvent (bottom). Reprinted from ref. 48 with permission from Wiley. (b) FTIR spectra of $FAPbBr_3$/DMSO solution after light soaking for different periods. (c) Current density–voltage (J–V) characteristics of mixed cation perovskite devices with different perovskite solution aging history. Reprinted from ref. 122 with permission from the American Chemical Society.

recombination centers.[121] As shown in Fig. 9(a), the color change of the mixed MA^+/FA^+ containing precursor solutions was more rapid than that of only $FAPbI_3$ perovskite precursor solutions.[48] Considering the deprotonation of MA^+ ions in the DMSO containing precursor solution as mentioned in Section 4.1.1, it is reasonable to speculate that over-stoichiometric I^- ions due to the loss of volatile CH_3NH_2 are more prone to easily oxidize to I_2, which deviate from the accurate stoichiometric ratio of precursors in the precursor solution.

Besides, light-induced FA^+ ion degradation in perovskite precursor solutions is also reported. Wei and co-workers found that a redox reaction between the –CH=NH bonds in FA^+ and $PbBr_2$ in a Br^- ion based precursor solution took place under illumination.[122] As a result, Pb^{2+} ions were reduced to Pb metal, and –CH=NH bonds were oxidized to –CH=O bonds as irreversible degradation (Fig. 9(b)). In contrast, the MA^+ ions were much more stable in the precursor solutions due to the absence of more reactive –CN=NH double bonds. However, under I^- ion abundant conditions, photoinduced decomposition of PbI_2 was observed in both MA^+ and mixed $Cs/MA^+/FA^+$ containing precursor solutions, leading to the generation of iodine, which changed the color of the precursor solutions to dark red after 5 h, and then the produced iodine would further serve as a catalyst in the redox reaction to activate the transformation of –CH=NH double bonds into –CH=O bonds in FA^+. Note that no such oxidization of FA^+ ions in solid films was observed. As expected, the PCE of $MAPbI_3$ based PSCs dropped from 19.6 to 15.6% due to the iodine interstitials or iodine vacancies in perovskite films after light soaking the precursor solution for 96 h, while it reduced from 19.5 to 14.3% for mixed $Cs/MA^+/FA^+$ based PSCs under a synergy effect between generated iodine and degraded –C=O molecules (Fig. 9(c)).

4.2.3 Hydrolysis. Great efforts have been devoted to the study of amide hydrolysis in biological systems and organic chemistry.[123,124] As the most typically used solvent in the preparation of perovskite precursor solution, DMF is known to undergo hydrolysis as shown in eqn (4)

$$HCON(CH_3)_2 \xleftrightarrow{H_2O} HCOOH + (CH_3)_2NH \quad (4)$$

and produce formic acid (HCOOH) and DMA.[123–125] It has been found that the hydrolysis of DMF could even be induced by a trace amount of water,[126] which occurs on both free and coordinated species. DMA^+ ions have been demonstrated to incorporate into perovskite structures and modify the perovskite film stoichiometry by a reduction of organic cations in the A sites of perovskite, yielding a yellowish δ-$FAPbI_3$ perovskite film with poor optoelectronic properties (Fig. 10(a–c)), while another hydrolysis product of HCOOH could escape from the film during annealing. With the help of highly sensitive time-of-flight secondary ion mass spectrometry (TOF-SIMS) and X-ray photoelectron spectroscopy (XPS), Lee and co-workers revealed that the extent of DMA levels in perovskite films ranges from roughly 10 to 50% depending on the environment and annealing conditions.[127] Considering as much as 50% DMA could cause a measurable peak shift of 0.1° in normal XRD measurement due to the similar size compared with FA, they highlighted that 10% DMA in perovskite could easily hide in high-performance solar cells.

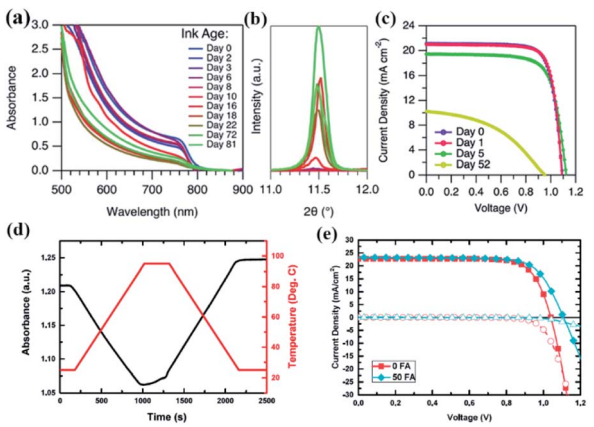

Fig. 10 (a) Absorption spectra and (b) selected XRD patterns (not normalized) of FAMAC films fabricated from FAMAC ink that was stored for different days in the dark in N_2. (c) Open-circuit voltage to short-circuit current scanned (reserve scan) J–V curves for the PSCs fabricated with FAMAC ink stored for different times: fresh ink and 1, 5, and 52 days. Reprinted from ref. 126 with permission from the American Chemical Society. (d) Evolution of the absorbance of thymol blue in DMF at 402 nm with time and temperature. The change in absorbance is depicted by the solid black line and the corresponding temperature curve is shown by the dashed red line. (e) Current–voltage curves of solar cells fabricated using neat DMF as a solvent, as well as DMF with 5 vol% of formic acid added. Solid symbols represent the light JV measurement, while hollow symbols show the dark JV measurement. Reprinted from ref. 129 with permission from Elsevier Inc.

Moreover, the hydrolysis products change the pH of the precursor solution, which has been proven as one of the crucial parameters that significantly impacts the perovskite crystallization kinetics and optoelectronic properties of the perovskite films.[128] Anhydrous DMF is a relatively neutral solvent with a pH of 6.3. Considering that the hydrolysis product of HCOOH is an acid and DMA is a base, both of which present in similar concentrations, the pH of hydrolyzed DMF solution depends on the pK_a of the products; the lower pK_a of DMA indicates that DMA is a stronger base and has a larger influence of the pH value. So, the hydrolyzed DMF tends to more basic. As shown in Fig. 10(d), by using thymol blue as a pH indicator in DMF, Noel and co-workers investigated the changes in pH during DMF hydrolysis at different temperatures and identified their impacts on the chemical properties of the perovskite precursor solution.[129] When increasing the solution temperature to 95 °C, the equilibria of the hydrolysis reaction moved to the product side, and a decreased basicity was observed due to the encouraging dissociation of HCOOH at elevated temperature. Then gradually cooled the solution back down to room temperature, the hydrolyzed DMF solution became increasingly basic and even more than in its initial pH value. The authors suggested that the produced DMA through hydrolysis can increase the solvating power of DMF to solvate the perovskite precursor salts, leading to an enhanced perovskite film quality. By employing formic acid (FA) to artificially tune the age of the DMF, an increased PCE was achieved compared to the device fabricated from the neat precursor solution (Fig. 10(e)).

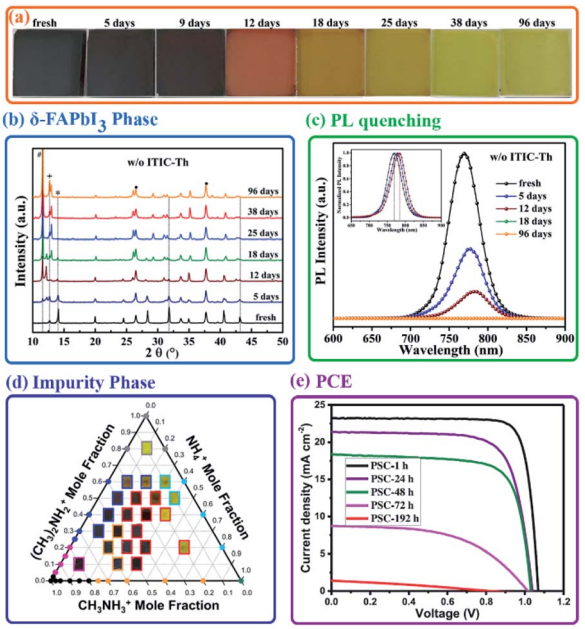

Fig. 11 (a) A series of photographs of perovskite films fabricated from perovskite precursor solutions aged for different amounts of time. The corresponding XRD (b) and PL spectra (c) of the perovskite films. Reprinted from ref. 130 with permission from Wiley. (d) Partial ternary phase diagram of $[DMA]_x(NH_4)_yMA_{1-x-y}PbI_3$. Photographs of triple organic cation films are overlaid on the corresponding data points in the center of the phase diagram. Reprinted from ref. 106 with permission from the American Chemical Society. (e) *I*–*V* curves and distribution of the PCE of PSCs fabricated as a function of the aging time of the precursor solution. Reprinted from ref. 48 with permission from Wiley.

4.3 Effects on the perovskite film quality

The degradation of perovskite precursor solutions not only reduces the reproducibility of film fabrication but also deteriorates the perovskite film performance. Fig. 11(a–e) summarizes the effects of the degradation of precursor solutions on the performance of the corresponding films and PSCs. Firstly, changes in the crystal phase transition were commonly observed. It can be seen that the black mixed organic cation perovskite films gradually faded out to light yellow with the precursor solution aging time.[130] The appearance of the diffraction peak at 11.7° with increasing aging time confirmed the formation of the hexagonal δ-phase of $FAPbI_3$ induced by the stored precursor solution. The phase transition of δ-$FAPbI_3$ to α-$FAPbI_3$ is known to occur in the case of FA^+ with a mixture of a certain amount of MA^+; the reverse transition suggests the reduced content of MA^+, and this may be related to the loss of MA^+ through the deprotonation of MA^+ to volatile CH_3NH_2 or the substitution of hydrolysis products of DMF in the perovskite structure discussed above. In addition, as shown in Fig. 11(c), PL quenching for perovskite films obtained from the stored precursor solutions was also observed, consistent with the formation of photoinactive δ-$FAPbI_3$. Secondly, the reaction byproducts with a comparable molecule size from solute–solvent and solute–solute reactions and the hydrolysis of DMF were found to incorporate into the perovskite structure as A-site impurities and resulted in some impurity phases, which have significant effects on the stoichiometry and optical properties of the perovskite films. For example, Fig. 11(d) exhibits the ternary phase diagram of the alloying of the solute–solvent reaction products (NH_4^+ and DMA^+) and MA^+ in the perovskite structure, and perovskite films with different components and optical properties can be obtained.[106] Moreover, the incorporated NH_4^+ and DMA^+ in the perovskite structure were found to induce a significant density of occupied states in the band gap of $MAPbI_3$ and limit the excursion of the Fermi level at the perovskite surface.[113] Finally, the PCEs of devices derived from the precursor solution show a rapid reduction to 75% of the initial value (20.82%) after storing for 72 h (Fig. 11(e)).[48]

4.4 Stabilization of the perovskite precursor solution

A few studies have tried to enhance the interaction between perovskite precursors and additives, to inhibit the chemical reactions between the solute and solvent mentioned above. The organic molecules of 3,9-bis(2-methylene-(3-(1,1-dicyanomethylene)-indanone))-5,5,11,11-tetrakis(5-hexylthienyl)-dithieno[2,3-*d*:2′,3′-*d*′]-*s*-indaceno[1,2-*b*:5,6-*b*′]dithiophene (ITIC-Th) and 1,4,7,10,13,16-hexaoxacyclooctadecane (18C6) have been incorporated into mixed cation perovskite precursor solutions to stabilize the perovskite precursor solution, in which the S in ITIC-Th and O in 18C6 were confirmed to form coordination or covalent bonds with Pb^{2+}, respectively.[130,131] Such bonding resulted in a more stable colloidal $[PbI_6]^{4-}$

framework and suppressed the formation of δ-$FAPbI_3$, which significantly prolonged the lifetime of precursor solutions for more than one month.

To further suppress the reaction byproducts originating from the deprotonation of MAI as impurities in the perovskite structure, the stabilizer triethyl borate (TEB) with electron-withdrawing capability has been demonstrated to form a strong interaction with I^- of MAI and reduce the electron cloud density of I^-, making it hard to capture the proton in MA^+ and efficiently inhibit the deprotonation of MAI.[107] As a result, the applied window period of the precursor solution was widened for more than 24 h, and only 4% FAI was confirmed to form byproduct MFAI after aging for 7 days, compared to that of 75% for the normal precursor solution. A similar interaction strategy was reported by incorporating elemental sulfur into precursor solutions.[48] The elemental sulfur exists as stable S_8 rings in the precursor solution and forms a complex with MA^+ by chemically interacting with the amine group. The complex could inhibit the volatilization of CH_3NH_2 and drastically improve the stability of the perovskite precursor solutions; the α-$FAPbI_3$ phase was retained and no visible δ-$FAPbI_3$ could be observed in the perovskite films prepared with the sulfur-containing precursor solution even after more than one week. Nevertheless, an alternative way is to decrease the MAI concentration or replace cesium or FAI in the DMSO and MAI containing perovskite precursor solution, which is suggested to essentially suppress the detrimental impact on the quality of perovskite films.[113]

Except for the suppression of chemical reactions in precursor solutions, the precursor solution degradation induced by environmental factors should also be avoided. For example, various additives, including hypophosphorous acid (HPA),[121] methylamine (CH_3NH_2),[132] formamidine acetate (FAAc),[128] and elemental sulfur (S_8),[48] have been developed to eliminate the oxidized I_2 in the precursor solutions. It was reported that the addition of CH_3NH_2 into the precursor solution effectively avoided the formation of oxidized I_2 and the disturbance of Pb/I stoichiometry, and the defect density of the perovskite film derived from the suppressed I_2 precursor solution decreased from 1.38×10^{16} to 1.5×10^{15} cm^3, and a PCE of 20.02% with a stabilized output efficiency of 19.01% was achieved for the PSCs based on the thick perovskite film with a thickness of ~650 nm. Besides, a solvent-less storage strategy was reported to avoid the modulation of the composition and crystal phase of the resulting perovskite films by the hydrolysis of DMF.[126] By utilizing a ball mill to uniformly mix the precursor salts into a mixed perovskite powder with desired stoichiometry, it can be dissolved in solvents immediately before use. Perovskite films prepared from the powder show no significant changes in either the structure or the optical properties after storing for 31 days.

5. Humidity effect on perovskite formation

Although the chemical species in perovskite precursor solutions plays a critical role in perovskite formation, as discussed in Section 2.2.1, solvated gel complexes precipitated from the perovskite precursor solution during solidification are directly related to the subsequent perovskite crystallization as well as the quality of perovskite films.[133,134] However, the gel complexes are metastable and sensitive to humidity since H_2O has a stronger bond affinity towards PbI_2 compared to the solvents in gel complexes, making it easy to coordinate with Pb^{2+} and suppress the formation of higher iodoplumbate complexes required for perovskite formation.[135] As a result, the stoichiometric ratio of PbI_2 and DMSO in precursor solutions needs to be carefully adjusted to achieve perovskite films with a desired morphology under different relative humidity conditions. Although a suitable amount of H_2O was reported as an additive to improve the quality of perovskite films,[136–138] unintentional moisture incursion can mediate the chemical species of the gel complexes and change the perovskite crystallization kinetics. In addition, the H_2O molecule has a strong hydrogen bonding interaction with DMF or DMSO. It can break the Pb–O bond in solvated complexes and attenuate the complexation of Pb^{2+} in gel complexes by reducing the availability of solvents.[139] Therefore, it is important to understand the underlying mechanism of the humidity effect on the chemical species of the gel complexes and further improve the reproducibility window for the future industrial fabrication of PSCs. In a very recent study shown in Fig. 12(a), the calculated and experimental results showed that one dimensional (1D) $PbI_2 \cdot 2DMSO$ is quickly formed due to the strong coordination of DMSO to Pb^{2+} after

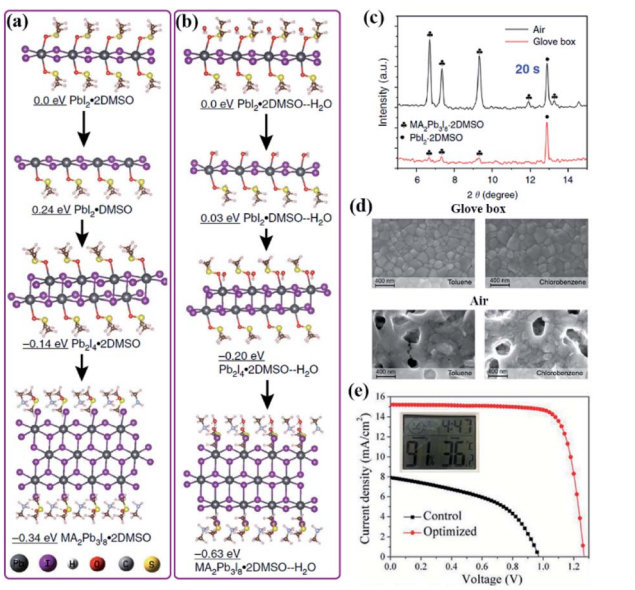

Fig. 12 Calculated structures and electronic energies of lead complexes without (a) and with H_2O (b). (c) The X-ray diffraction patterns (XRD) of Pb-complex films fabricated in ambient air and in a glove box with a sample spinning time of 20 s. Reprinted from ref. 140 with permission from the Nature Publishing group. (d) SEM images of perovskite films fabricated with different antisolvents—the commonly used are toluene and chlorobenzene. Reprinted from ref. 139 with permission from Wiley. (e) *J*–*V* curves of the control and optimized $CsPbI_2Br$ PSCs prepared in air with a high RH of 91% and temperature of 36 °C. Reprinted from ref. 141 with permission from Wiley.

mixing MAI/PbI_2 in the DMF/DMSO mixed solution, and then they combine together and further convert to $Pb_2I_4 \cdot 2DMSO$ and $MA_2Pb_3I_8 \cdot 2DMSO$, driven by the concentration of the precursor.[140] However, H_2O will interact with DMSO in these lead complexes and reduce their relative electronic energies in a way (Fig. 12(b)), thus facilitating the conversion from the 1D $H_2O \cdot PbI_2 \cdot 2DMSO$ lead complex to 1D $MA_2Pb_3I_8 \cdot 2DMSO$ with much longer needle-like fibers in the morphology than those grown in the water-free environment as confirmed by XRD patterns in Fig. 12(c). This is consistent with the reported moisture-induced crystal-growth anisotropy phenomenon under ambient conditions, where porous perovskite films can even be fabricated by an anti-solvent assisted method (Fig. 12(d)).[139]

Except for the humidity effect on hybrid perovskites, the fabrication of high-efficiency inorganic PSCs is known highly sensitive to moisture and is generally limited in an inert-filled glovebox or dry air atmosphere. Very recently, to suppress the effects of humidity and achieve the air fabrication process of inorganic PSCs, a new precursor system by mixing HCOOCs, $HPbI_3$, and $HPbBr_3$ was developed to replace the traditional precursor solutions commonly used for the fabrication of inorganic PSCs.[141] A new complex HCOOH–Cs^+ present in the precursor system was confirmed to prevent moisture incursion and protect the gel precursor films from an unwanted phase transition in ambient air. Finally, as shown in Fig. 12(e), an impressive PCE of 15.1% was achieved for inorganic PSCs in the atmosphere with 91% relative humidity. These results suggest that tailored iodoplumbate complexes in perovskite precursor solutions can be obtained through precursor engineering, which can achieve desired perovskite crystallization under various fabrication conditions and further improve the PSC performance.

6. Conclusions and outlook

In summary, we presented insights into the evolution of the characteristics of a perovskite precursor solution driven by the components of the precursor solution, aging effect, degradation effect, and humidity effect and revealed their impact on the physical properties of perovskite films and the PSC performance. Iodoplumbate complexes, such as PbI_2, PbI_3^-, and PbI_4^{2-}, are present in the perovskite precursor solution in equilibria and serve as precursors that dictate the quality of perovskite films and the optoelectrical performance of PSCs. The solvent and additive molecules are prone to compete with I^- to coordinate with Pb^{2+} due to their coordination capabilities, shifting the precursor equilibria to iodoplumbate complexes with a smaller number of I^- ions, thus controlling perovskite formation. As a result, the perovskite precursor solutions often need a special aging time, ranging from a few to several tens of hours to achieve the optimal performance of PSCs. The status of the precursor solution continuously evolves and will have a time-dependent influence on the quality of perovskite films until the solution reaches new equilibria. Then the efficiency of PSCs drops rapidly due to the degradation of the perovskite precursor solution induced by the chemical reactions between components or exposure to external stimuli. In addition, the PCEs of PSCs are also sensitive to the fabrication atmosphere since moisture can interact with either Pb^{2+} ions in gel complexes or solvent molecules to modify the subsequent perovskite crystallization kinetics, which further reduces the reproducibility of highly efficient PSCs. Based on the discussion above, we present the following suggestions to further improve the reproducibility of highly efficient PSCs:

(1) Increase the iodide coordination number in the coordination complexes present in the precursor solutions or gel precursor films before perovskite formation.

(2) Carefully adjust the optimal aging window for perovskite precursor solutions under different storage conditions.

(3) Avoid the degradation of precursor solutions induced by chemical reactions between the components and environmental conditions.

(4) Prevent unintentional moisture incursion during perovskite formation.

(5) Tailor iodoplumbate complexes in perovskite precursor solutions through precursor engineering to meet the various fabrication conditions.

Although excellent progress has been made in understanding the relationships between the characteristics of the perovskite precursor solution and the reproducibility of high-quality perovskite films and improvement of the efficiency of PSCs, the effect of precursor aging on the reproducibility of highly efficient PSCs is intractable, which needs to be carefully considered. The aging of the perovskite precursor could benefit the quality of the resultant perovskite film. However, long-term storage (or exposure to external stimuli) may lead to the degradation of the precursor and deteriorate the perovskite film. Efforts towards stabilizing the perovskite precursor solution and in-depth understanding of the degradation mechanism of the precursor are still required. Tailoring the perovskite precursor solution with weak coordination solvents may promote the complexation of Pb^{2+} and I^- to form sufficient high order iodoplumbate complexes that are required for perovskite formation, which may suppress the effect of the precursor solution aging to facilitate the formation of highly reproducible perovskite films.

Conflicts of interest

There are no conflicts to declare.

Acknowledgements

This work was supported by the National Key Research and Development Program of China (2017YFE0119700), National Natural Science Foundation of China (51961135107, 51774034, 51772026, and 51672208), Beijing Natural Science Foundation (2182039), and Open Foundation Project of Key Laboratory of Plateau Green Building and Ecological Community of Qinghai Province (KLKF-2019-002).

References

1 D. Weber, *Z. Naturforsch. B*, 1978, **33**, 1443–1445.

2 D. B. Mitzi, *J. Mater. Chem.*, 2004, **14**, 2355–2365.
3 M. I. Saidaminov, K. Williams, M. Wei, A. Johnston, R. Quintero-Bermudez, M. Vafaie, J. M. Pina, A. H. Proppe, Y. Hou, G. Walters, S. O. Kelley, W. A. Tisdale and E. H. Sargent, *Nat. Mater.*, 2020, **19**, 412–418.
4 E. M. Hutter, M. C. Gelvez-Rueda, A. Osherov, V. Bulovic, F. C. Grozema, S. D. Stranks and T. J. Savenije, *Nat. Mater.*, 2017, **16**, 115–120.
5 J. H. Noh, S. H. Im, J. H. Heo, T. N. Mandal and S. I. Seok, *Nano Lett.*, 2013, **13**, 1764–1769.
6 H. S. Kim, C. R. Lee, J. H. Im, K. B. Lee, T. Moehl, A. Marchioro, S. J. Moon, R. Humphry-Baker, J. H. Yum, J. E. Moser, M. Gratzel and N. G. Park, *Sci. Rep.*, 2012, **2**, 591.
7 S. De Wolf, J. Holovsky, S.-J. Moon, P. Löper, B. Niesen, M. Ledinsky, F.-J. Haug, J.-H. Yum and C. Ballif, *J. Phys. Chem. Lett.*, 2014, **5**, 1035–1039.
8 V. D'Innocenzo, G. Grancini, M. J. Alcocer, A. R. Kandada, S. D. Stranks, M. M. Lee, G. Lanzani, H. J. Snaith and A. Petrozza, *Nat. Commun.*, 2014, **5**, 3586.
9 J. Huang, Y. Yuan, Y. Shao and Y. Yan, *Nat. Rev. Mater.*, 2017, **2**, 17042.
10 M. Li, B. Li, G. Cao and J. Tian, *J. Mater. Chem. A*, 2017, **5**, 21313–21319.
11 S. D. Stranks, G. E. Eperon, G. Grancini, C. Menelaou, M. J. Alcocer, T. Leijtens, L. M. Herz, A. Petrozza and H. J. Snaith, *Science*, 2013, **342**, 341–344.
12 M. Wang, B. Li, P. Siffalovic, L.-C. Chen, G. Cao and J. Tian, *J. Mater. Chem. A*, 2018, **6**, 15386–15394.
13 B. Li, M. J. Li, C. B. Fei, G. Z. Cao and J. J. Tian, *J. Mater. Chem. A*, 2017, **5**, 24168–24177.
14 D. T. Moore, H. Sai, K. W. Tan, D. M. Smilgies, W. Zhang, H. J. Snaith, U. Wiesner and L. A. Estroff, *J. Am. Chem. Soc.*, 2015, **137**, 2350–2358.
15 S. Yun, Y. Zhang, Q. Xu, J. Liu and Y. Qin, *Nano Energy*, 2019, **60**, 600–619.
16 A. Kojima, K. Teshima, Y. Shirai and T. Miyasaka, *J. Am. Chem. Soc.*, 2009, **131**, 6050–6051.
17 S. Yun, N. Vlachopoulos, A. Qurashi, S. Ahmad and A. Hagfeldt, *Chem. Soc. Rev.*, 2019, **48**, 3705–3722.
18 W. S. Yang, J. H. Noh, N. J. Jeon, Y. C. Kim, S. Ryu, J. Seo and S. I. Seok, *Science*, 2015, **348**, 1234–1237.
19 X. Li, D. Bi, C. Yi, J.-D. Décoppet, J. Luo, S. M. Zakeeruddin, A. Hagfeldt and M. Grätzel, *Science*, 2016, aaf8060.
20 H. Tan, A. Jain, O. Voznyy, X. Lan, F. P. Garcia de Arquer, J. Z. Fan, R. Quintero-Bermudez, M. Yuan, B. Zhang, Y. Zhao, F. Fan, P. Li, L. N. Quan, Y. Zhao, Z. H. Lu, Z. Yang, S. Hoogland and E. H. Sargent, *Science*, 2017, **355**, 722–726.
21 E. H. Jung, N. J. Jeon, E. Y. Park, C. S. Moon, T. J. Shin, T.-Y. Yang, J. H. Noh and J. Seo, *Nature*, 2019, **567**, 511–515.
22 S. Yang, S. Chen, E. Mosconi, Y. Fang, X. Xiao, C. Wang, Y. Zhou, Z. Yu, J. Zhao, Y. Gao, F. De Angelis and J. Huang, *Science*, 2019, **365**, 473–478.
23 H. Lu, Y. Liu, P. Ahlawat, A. Mishra, W. R. Tress, F. T. Eickemeyer, Y. Yang, F. Fu, Z. Wang, C. E. Avalos, B. I. Carlsen, A. Agarwalla, X. Zhang, X. Li, Y. Zhan, S. M. Zakeeruddin, L. Emsley, U. Rothlisberger, L. Zheng, A. Hagfeldt and M. Gratzel, *Science*, 2020, **370**, eabb8985.
24 S. Yun, Y. Qin, A. R. Uhl, N. Vlachopoulos, M. Yin, D. Li, X. Han and A. Hagfeldt, *Energy Environ. Sci.*, 2018, **11**, 476–526.
25 NREL, https://www.nrel.gov/pv/assets/images/efficiency-chart.png, accessed, January 2021.
26 C. Fei, B. Li, R. Zhang, H. Fu, J. Tian and G. Cao, *Adv. Energy Mater.*, 2017, **7**, 1602017.
27 M. Yang, Z. Li, M. O. Reese, O. G. Reid, D. H. Kim, S. Siol, T. R. Klein, Y. Yan, J. J. Berry, M. F. A. M. van Hest and K. Zhu, *Nat. Energy*, 2017, **2**, 17038.
28 L. Li, N. Liu, Z. Xu, Q. Chen, X. Wang and H. Zhou, *ACS Nano*, 2017, **11**, 8804–8813.
29 J. Kim, B. W. Park, J. Baek, J. S. Yun, H. W. Kwon, J. Seidel, H. Min, S. Coelho, S. Lim, S. Huang, K. Gaus, M. A. Green, T. J. Shin, A. W. Y. Ho-Baillie, M. G. Kim and S. I. Seok, *J. Am. Chem. Soc.*, 2020, **142**, 6251–6260.
30 K. Yan, M. Long, T. Zhang, Z. Wei, H. Chen, S. Yang and J. Xu, *J. Am. Chem. Soc.*, 2015, **137**, 4460–4468.
31 J. S. Manser, M. I. Saidaminov, J. A. Christians, O. M. Bakr and P. V. Kamat, *Acc. Chem. Res.*, 2016, **49**, 330–338.
32 B. Li, D. Binks, G. Cao and J. Tian, *Small*, 2019, **15**, e1903613.
33 M. Jung, S. G. Ji, G. Kim and S. I. Seok, *Chem. Soc. Rev.*, 2019, **48**, 2011–2038.
34 Y. Guo, K. Shoyama, W. Sato, Y. Matsuo, K. Inoue, K. Harano, C. Liu, H. Tanaka and E. Nakamura, *J. Am. Chem. Soc.*, 2015, **137**, 15907–15914.
35 S. A. Fateev, A. A. Petrov, V. N. Khrustalev, P. V. Dorovatovskii, Y. V. Zubavichus, E. A. Goodilin and A. B. Tarasov, *Chem. Mater.*, 2018, **30**, 5237–5244.
36 X. Huang, R. Chen, G. Deng, F. Han, P. Ruan, F. Cheng, J. Yin, B. Wu and N. Zheng, *J. Am. Chem. Soc.*, 2020, **142**, 6149–6157.
37 J. C. Hamill, J. Schwartz and Y.-L. Loo, *ACS Energy Lett.*, 2017, **3**, 92–97.
38 G. S. Shin, S. G. Kim, Y. Zhang and N. G. Park, *Small Methods*, 2019, **4**, 1900398.
39 H. Tsai, W. Nie, Y.-H. Lin, J. C. Blancon, S. Tretiak, J. Even, G. Gupta, P. M. Ajayan and A. D. Mohite, *Adv. Energy Mater.*, 2017, **7**, 1602159.
40 D. P. McMeekin, Z. Wang, W. Rehman, F. Pulvirenti, J. B. Patel, N. K. Noel, M. B. Johnston, S. R. Marder, L. M. Herz and H. J. Snaith, *Adv. Mater.*, 2017, **29**, 1607039.
41 M. Xiao, F. Huang, W. Huang, Y. Dkhissi, Y. Zhu, J. Etheridge, A. Gray-Weale, U. Bach, Y. B. Cheng and L. Spiccia, *Angew. Chem., Int. Ed.*, 2014, **53**, 10056–10061.
42 F. Li, C. Bao, H. Gao, W. Zhu, T. Yu, J. Yang, G. Fu, X. Zhou and Z. Zou, *Mater. Lett.*, 2015, **157**, 38–41.
43 S. H. Huang, C. K. Guan, P. H. Lee, H. C. Huang, C. F. Li, Y. C. Huang and W. F. Su, *Adv. Energy Mater.*, 2020, **10**, 2001567.
44 Y. Zhong, R. Munir, J. Li, M.-C. Tang, M. R. Niazi, D.-M. Smilgies, K. Zhao and A. Amassian, *ACS Energy Lett.*, 2018, **3**, 1078–1085.

45 C. Li, J. Yin, R. Chen, X. Lv, X. Feng, Y. Wu and J. Cao, *J. Am. Chem. Soc.*, 2019, **141**, 6345–6351.
46 Z. Wei, H. Chen, K. Yan and S. Yang, *Angew. Chem., Int. Ed.*, 2014, **53**, 13239–13243.
47 F. Mathies, T. Abzieher, A. Hochstuhl, K. Glaser, A. Colsmann, U. W. Paetzold, G. Hernandez-Sosa, U. Lemmer and A. Quintilla, *J. Mater. Chem. A*, 2016, **4**, 19207–19213.
48 H. Min, G. Kim, M. J. Paik, S. Lee, W. S. Yang, M. Jung and S. I. Seok, *Adv. Energy Mater.*, 2019, **9**, 1803476.
49 Y. Zhou, O. S. Game, S. Pang and N. P. Padture, *J. Phys. Chem. Lett.*, 2015, **6**, 4827–4839.
50 H. Miyamae, H. Toriyama, T. Abe, G. Hihara and M. Nagata, *Acta Crystallogr., Sect. C: Cryst. Struct. Commun.*, 1984, **40**, 1559–1562.
51 J. Parr, *Polyhedron*, 1997, **16**, 551–566.
52 O. E. Lanford and S. J. Kiehl, *J. Am. Chem. Soc.*, 1941, **63**, 667–669.
53 K. G. Stamplecoskie, J. S. Manser and P. V. Kamat, *Energy Environ. Sci.*, 2015, **8**, 208–215.
54 A. Sharenko, C. Mackeen, L. Jewell, F. Bridges and M. F. Toney, *Chem. Mater.*, 2017, **29**, 1315–1320.
55 E. Radicchi, E. Mosconi, F. Elisei, F. Nunzi and F. De Angelis, *ACS Appl. Energy Mater.*, 2019, **2**, 3400–3409.
56 P. Ahlawat, M. I. Dar, P. Piaggi, M. Grätzel, M. Parrinello and U. Rothlisberger, *Chem. Mater.*, 2019, **32**, 529–536.
57 Q. Hu, L. Zhao, J. Wu, K. Gao, D. Luo, Y. Jiang, Z. Zhang, C. Zhu, E. Schaible, A. Hexemer, C. Wang, Y. Liu, W. Zhang, M. Gratzel, F. Liu, T. P. Russell, R. Zhu and Q. Gong, *Nat. Commun.*, 2017, **8**, 15688.
58 N. Ahn, D. Y. Son, I. H. Jang, S. M. Kang, M. Choi and N. G. Park, *J. Am. Chem. Soc.*, 2015, **137**, 8696–8699.
59 N. J. Jeon, J. H. Noh, Y. C. Kim, W. S. Yang, S. Ryu and S. I. Seok, *Nat. Mater.*, 2014, **13**, 897–903.
60 F. Cai, Y. Yan, J. Yao, P. Wang, H. Wang, R. S. Gurney, D. Liu and T. Wang, *Adv. Funct. Mater.*, 2018, **28**, 1801985.
61 J. Kim, M. I. Saidaminov, H. Tan, Y. Zhao, Y. Kim, J. Choi, J. W. Jo, J. Fan, R. Quintero-Bermudez, Z. Yang, L. N. Quan, M. Wei, O. Voznyy and E. H. Sargent, *Adv. Mater.*, 2018, **30**, e1706275.
62 J.-Y. Seo, T. Matsui, J. Luo, J.-P. Correa-Baena, F. Giordano, M. Saliba, K. Schenk, A. Ummadisingu, K. Domanski, M. Hadadian, A. Hagfeldt, S. M. Zakeeruddin, U. Steiner, M. Grätzel and A. Abate, *Adv. Energy Mater.*, 2016, **6**, 1600767.
63 Y. Rong, Z. Tang, Y. Zhao, X. Zhong, S. Venkatesan, H. Graham, M. Patton, Y. Jing, A. M. Guloy and Y. Yao, *Nanoscale*, 2015, **7**, 10595–10599.
64 L. Chao, Y. Xia, B. Li, G. Xing, Y. Chen and W. Huang, *Chem*, 2019, **5**, 995–1006.
65 S. Rahimnejad, A. Kovalenko, S. M. Fores, C. Aranda and A. Guerrero, *ChemPhysChem*, 2016, **17**, 2795–2798.
66 X. Guo, C. McCleese, C. Kolodziej, A. C. S. Samia, Y. Zhao and C. Burda, *Dalton Trans.*, 2016, **45**, 3806–3813.
67 S. Bae, S. J. Han, T. J. Shin and W. H. Jo, *J. Mater. Chem. A*, 2015, **3**, 23964–23972.
68 A. A. Petrov, I. P. Sokolova, N. A. Belich, G. S. Peters, P. V. Dorovatovskii, Y. V. Zubavichus, V. N. Khrustalev, A. V. Petrov, M. Grätzel, E. A. Goodilin and A. B. Tarasov, *J. Phys. Chem. C*, 2017, **121**, 20739–20743.
69 K. H. Hendriks, J. J. van Franeker, B. J. Bruijnaers, J. A. Anta, M. M. Wienk and R. A. J. Janssen, *J. Mater. Chem. A*, 2017, **5**, 2346–2354.
70 Y. Xia, C. Ran, Y. Chen, Q. Li, N. Jiang, C. Li, Y. Pan, T. Li, J. Wang and W. Huang, *J. Mater. Chem. A*, 2017, **5**, 3193–3202.
71 Y. Wu, F. Xie, H. Chen, X. Yang, H. Su, M. Cai, Z. Zhou, T. Noda and L. Han, *Adv. Mater.*, 2017, **29**, 1701073.
72 L. Zhang, B. Li, J. Yuan, M. Wang, T. Shen, F. Huang, W. Wen, G. Cao and J. Tian, *J. Phys. Chem. Lett.*, 2018, **9**, 3646–3653.
73 Y. Bai, S. Xiao, C. Hu, T. Zhang, X. Meng, Q. Li, Y. Yang, K. S. Wong, H. Chen and S. Yang, *Nano Energy*, 2017, **34**, 58–68.
74 F. Huang, Y. Dkhissi, W. Huang, M. Xiao, I. Benesperi, S. Rubanov, Y. Zhu, X. Lin, L. Jiang, Y. Zhou, A. Gray-Weale, J. Etheridge, C. R. McNeill, R. A. Caruso, U. Bach, L. Spiccia and Y.-B. Cheng, *Nano Energy*, 2014, **10**, 10–18.
75 B. Li, Q. Zhang, S. Zhang, Z. Ahmad, T. Chidanguro, A. Hunter Davis, Y. C. Simon, X. Gu, W. Zheng, N. Pradhan and Q. Dai, *Chem. Eng. J.*, 2021, **405**, 126998.
76 Y. Li, Z. Zhao, F. Lin, X. Cao, X. Cui and J. Wei, *Small*, 2017, **13**, 1604125.
77 Y. C. Zheng, S. Yang, X. Chen, Y. Chen, Y. Hou and H. G. Yang, *Chem. Mater.*, 2015, **27**, 5116–5121.
78 B. Li, C. Fei, K. Zheng, X. Qu, T. Pullerits, G. Cao and J. Tian, *J. Mater. Chem. A*, 2016, **4**, 17018–17024.
79 Q. Han, Y. Bai, J. Liu, K.-z. Du, T. Li, D. Ji, Y. Zhou, C. Cao, D. Shin, J. Ding, A. D. Franklin, J. T. Glass, J. Hu, M. J. Therien, J. Liu and D. B. Mitzi, *Energy Environ. Sci.*, 2017, **10**, 2365–2371.
80 Z. Xu, Z. Liu, N. Li, G. Tang, G. Zheng, C. Zhu, Y. Chen, L. Wang, Y. Huang, L. Li, N. Zhou, J. Hong, Q. Chen and H. Zhou, *Adv. Mater.*, 2019, **31**, e1900390.
81 Z. Wang, Y. Zhou, S. Pang, Z. Xiao, J. Zhang, W. Chai, H. Xu, Z. Liu, N. P. Padture and G. Cui, *Chem. Mater.*, 2015, **27**, 7149–7155.
82 T. Bu, X. Liu, Y. Zhou, J. Yi, X. Huang, L. Luo, J. Xiao, Z. Ku, Y. Peng, F. Huang, Y.-B. Cheng and J. Zhong, *Energy Environ. Sci.*, 2017, **10**, 2509–2515.
83 M. Saliba, T. Matsui, J.-Y. Seo, K. Domanski, J.-P. Correa-Baena, M. K. Nazeeruddin, S. M. Zakeeruddin, W. Tress, A. Abate, A. Hagfeldt and M. Grätzel, *Energy Environ. Sci.*, 2016, **9**, 1989–1997.
84 M. Abdi-Jalebi, Z. Andaji-Garmaroudi, S. Cacovich, C. Stavrakas, B. Philippe, J. M. Richter, M. Alsari, E. P. Booker, E. M. Hutter, A. J. Pearson, S. Lilliu, T. J. Savenije, H. Rensmo, G. Divitini, C. Ducati, R. H. Friend and S. D. Stranks, *Nature*, 2018, **555**, 497–501.
85 D. Y. Son, S. G. Kim, J. Y. Seo, S. H. Lee, H. Shin, D. Lee and N. G. Park, *J. Am. Chem. Soc.*, 2018, **140**, 1358–1364.
86 C. Liang, H. Gu, Y. Xia, Z. Wang, X. Liu, J. Xia, S. Zuo, Y. Hu, X. Gao, W. Hui, L. Chao, T. Niu, M. Fang, H. Lu, H. Dong,

H. Yu, S. Chen, X. Ran, L. Song, B. Li, J. Zhang, Y. Peng, G. Shao, J. Wang, Y. Chen, G. Xing and W. Huang, *Nat. Energy*, 2020, **6**, 38–45.

87 H. Tsai, W. Nie, J. C. Blancon, C. C. Stoumpos, R. Asadpour, B. Harutyunyan, A. J. Neukirch, R. Verduzco, J. J. Crochet, S. Tretiak, L. Pedesseau, J. Even, M. A. Alam, G. Gupta, J. Lou, P. M. Ajayan, M. J. Bedzyk and M. G. Kanatzidis, *Nature*, 2016, **536**, 312–316.

88 E. Shi, Y. Gao, B. P. Finkenauer, Akriti, A. H. Coffey and L. Dou, *Chem. Soc. Rev.*, 2018, **47**, 6046–6072.

89 J. Hu, I. W. H. Oswald, S. J. Stuard, M. M. Nahid, N. Zhou, O. F. Williams, Z. Guo, L. Yan, H. Hu, Z. Chen, X. Xiao, Y. Lin, Z. Yang, J. Huang, A. M. Moran, H. Ade, J. R. Neilson and W. You, *Nat. Commun.*, 2019, **10**, 1276.

90 L. Liu, Y. Bai, X. Zhang, Y. Shang, C. Wang, H. Wang, C. Zhu, C. Hu, J. Wu, H. Zhou, Y. Li, S. Yang, Z. Ning and Q. Chen, *Angew. Chem., Int. Ed.*, 2020, **59**, 5979–5987.

91 J. P. Correa-Baena, Y. Luo, T. M. Brenner, J. Snaider, S. Sun, X. Li, M. A. Jensen, N. T. P. Hartono, L. Nienhaus, S. Wieghold, J. R. Poindexter, S. Wang, Y. S. Meng, T. Wang, B. Lai, M. V. Holt, Z. Cai, M. G. Bawendi, L. Huang, T. Buonassisi and D. P. Fenning, *Science*, 2019, **363**, 627–631.

92 S. Yun, X. Zhou, J. Even and A. Hagfeldt, *Angew. Chem., Int. Ed.*, 2017, **56**, 15806–15817.

93 D. Luo, R. Su, W. Zhang, Q. Gong and R. Zhu, *Nat. Rev. Mater.*, 2019, **5**, 44–60.

94 J. M. Ball and A. Petrozza, *Nat. Energy*, 2016, **1**, 16149.

95 W. S. Yang, B. W. Park, E. H. Jung, N. J. Jeon, Y. C. Kim, D. U. Lee, S. S. Shin, J. Seo, E. K. Kim, J. H. Noh and S. I. Seok, *Science*, 2017, **356**, 1376–1379.

96 R. J. Stewart, C. Grieco, A. V. Larsen, G. S. Doucette and J. B. Asbury, *J. Phys. Chem. C*, 2016, **120**, 12392–12402.

97 P. Boonmongkolras, D. Kim, E. M. Alhabshi, I. Gereige and B. Shin, *RSC Adv.*, 2018, **8**, 21551–21557.

98 W. Zhu, Q. Zhang, C. Zhang, Z. Zhang, D. Chen, Z. Lin, J. Chang, J. Zhang and Y. Hao, *ACS Appl. Energy Mater.*, 2018, **1**, 4991–4997.

99 J. S. Manser, B. Reid and P. V. Kamat, *J. Phys. Chem. C*, 2015, **119**, 17065–17073.

100 B. Li, F. H. Isikgor, H. Coskun and J. Ouyang, *Angew. Chem., Int. Ed.*, 2017, **56**, 16073–16076.

101 T. Li, Y. Pan, Z. Wang, Y. Xia, Y. Chen and W. Huang, *J. Mater. Chem. A*, 2017, **5**, 12602–12652.

102 Z. Huang, X. Hu, C. Liu, L. Tan and Y. Chen, *Adv. Funct. Mater.*, 2017, **27**, 1703061.

103 C. Fei, L. Guo, B. Li, R. Zhang, H. Fu, J. Tian and G. Cao, *Nano Energy*, 2016, **27**, 17–26.

104 B.-X. Chen, W.-G. Li, H.-S. Rao, Y.-F. Xu, D.-B. Kuang and C.-Y. Su, *Nano Energy*, 2017, **34**, 264–270.

105 J. Wang, F. Meng, R. Li, S. Chen, X. Huang, J. Xu, X. Lin, R. Chen, H. Wu and H.-L. Wang, *Sol. RRL*, 2020, **4**, 2000091.

106 J. C. Hamill, J. C. Sorli, I. Pelczer, J. Schwartz and Y.-L. Loo, *Chem. Mater.*, 2019, **31**, 2114–2120.

107 X. Wang, Y. Fan, L. Wang, C. Chen, Z. Li, R. Liu, H. Meng, Z. Shao, X. Du, H. Zhang, G. Cui and S. Pang, *Chem*, 2020, **6**, 1369–1378.

108 P. K. Nayak, D. T. Moore, B. Wenger, S. Nayak, A. A. Haghighirad, A. Fineberg, N. K. Noel, O. G. Reid, G. Rumbles, P. Kukura, K. A. Vincent and H. J. Snaith, *Nat. Commun.*, 2016, **7**, 13303.

109 M. I. Saidaminov, A. L. Abdelhady, B. Murali, E. Alarousu, V. M. Burlakov, W. Peng, I. Dursun, L. Wang, Y. He, G. Maculan, A. Goriely, T. Wu, O. F. Mohammed and O. M. Bakr, *Nat. Commun.*, 2015, **6**, 7586.

110 X. Cheng, S. Yang, B. Cao, X. Tao and Z. Chen, *Adv. Funct. Mater.*, 2019, **30**, 1905021.

111 Y. Chen, M. He, J. Peng, Y. Sun and Z. Liang, *Adv. Sci.*, 2016, **3**, 1500392.

112 M. De Bastiani, M. I. Saidaminov, I. Dursun, L. Sinatra, W. Peng, U. Buttner, O. F. Mohammed and O. M. Bakr, *Chem. Mater.*, 2017, **29**, 3367–3370.

113 F. Zhang, J. C. Hamill Jr, Y. L. Loo and A. Kahn, *Adv. Mater.*, 2020, **2**, e2003482.

114 D. Bryant, N. Aristidou, S. Pont, I. Sanchez-Molina, T. Chotchunangatchaval, S. Wheeler, J. R. Durrant and S. A. Haque, *Energy Environ. Sci.*, 2016, **9**, 1655–1660.

115 Y. Li, X. Xu, C. Wang, B. Ecker, J. Yang, J. Huang and Y. Gao, *J. Phys. Chem. C*, 2017, **121**, 3904–3910.

116 D. W. deQuilettes, W. Zhang, V. M. Burlakov, D. J. Graham, T. Leijtens, A. Osherov, V. Bulovic, H. J. Snaith, D. S. Ginger and S. D. Stranks, *Nat. Commun.*, 2016, **7**, 11683.

117 Y. C. Zhao, W. K. Zhou, X. Zhou, K. H. Liu, D. P. Yu and Q. Zhao, *Light: Sci. Appl.*, 2017, **6**, e16243.

118 A. Ummadisingu, L. Steier, J. Y. Seo, T. Matsui, A. Abate, W. Tress and M. Gratzel, *Nature*, 2017, **545**, 208–212.

119 G. Niu, W. Li, F. Meng, L. Wang, H. Dong and Y. Qiu, *J. Mater. Chem. A*, 2014, **2**, 705–710.

120 Z. Wang, Z. Shi, T. Li, Y. Chen and W. Huang, *Angew. Chem., Int. Ed.*, 2017, **56**, 1190–1212.

121 W. Zhang, S. Pathak, N. Sakai, T. Stergiopoulos, P. K. Nayak, N. K. Noel, A. A. Haghighirad, V. M. Burlakov, D. W. deQuilettes, A. Sadhanala, W. Li, L. Wang, D. S. Ginger, R. H. Friend and H. J. Snaith, *Nat. Commun.*, 2015, **6**, 10030.

122 H. Wei, S. Chen, J. Zhao, Z. Yu and J. Huang, *Chem. Mater.*, 2020, **32**, 2501–2507.

123 R. S. Brown, A. J. Bennet and H. Slebocka-Tilk, *Acc. Chem. Res.*, 2002, **25**, 481–488.

124 D. Zahn, *J. Phys. Chem. B*, 2003, **107**, 12303–12306.

125 T. Cottineau, M. Richard-Plouet, J.-Y. Mevellec and L. Brohan, *J. Phys. Chem. C*, 2011, **115**, 12269–12274.

126 B. Dou, L. M. Wheeler, J. A. Christians, D. T. Moore, S. P. Harvey, J. J. Berry, F. S. Barnes, S. E. Shaheen and M. F. A. M. van Hest, *ACS Energy Lett.*, 2018, **3**, 979–985.

127 M. V. Lee, S. R. Raga, Y. Kato, M. R. Leyden, L. K. Ono, S. Wang and Y. Qi, *J. Mater. Res.*, 2016, **32**, 45–55.

128 Y. Chen, N. Li, L. Wang, L. Li, Z. Xu, H. Jiao, P. Liu, C. Zhu, H. Zai, M. Sun, W. Zou, S. Zhang, G. Xing, X. Liu, J. Wang, D. Li, B. Huang, Q. Chen and H. Zhou, *Nat. Commun.*, 2019, **10**, 1112.

129 N. K. Noel, M. Congiu, A. J. Ramadan, S. Fearn, D. P. McMeekin, J. B. Patel, M. B. Johnston, B. Wenger and H. J. Snaith, *Joule*, 2017, **1**, 328–343.

130 M. Qin, J. Cao, T. Zhang, J. Mai, T.-K. Lau, S. Zhou, Y. Zhou, J. Wang, Y.-J. Hsu, N. Zhao, J. Xu, X. Zhan and X. Lu, *Adv. Energy Mater.*, 2018, **8**, 1703399.
131 X. Wu, Y. Jiang, C. Chen, J. Guo, X. Kong, Y. Feng, S. Wu, X. Gao, X. Lu, Q. Wang, G. Zhou, Y. Chen, J. M. Liu, K. Kempa and J. Gao, *Adv. Funct. Mater.*, 2019, **30**, 1908613.
132 Z. Liu, J. Hu, H. Jiao, L. Li, G. Zheng, Y. Chen, Y. Huang, Q. Zhang, C. Shen, Q. Chen and H. Zhou, *Adv. Mater.*, 2017, **29**, 1606774.
133 K. Meng, L. Wu, Z. Liu, X. Wang, Q. Xu, Y. Hu, S. He, X. Li, T. Li and G. Chen, *Adv. Mater.*, 2018, **30**, 1706401.
134 R. Munir, A. D. Sheikh, M. Abdelsamie, H. Hu, L. Yu, K. Zhao, T. Kim, O. E. Tall, R. Li, D. M. Smilgies and A. Amassian, *Adv. Mater.*, 2017, **29**, 1604113.
135 C. Aranda, C. Cristobal, L. Shooshtari, C. Li, S. Huettner and A. Guerrero, *Sustainable Energy Fuels*, 2017, **1**, 540–547.
136 C.-H. Chiang, M. K. Nazeeruddin, M. Grätzel and C.-G. Wu, *Energy Environ. Sci.*, 2017, **10**, 808–817.
137 X. Gong, M. Li, X.-B. Shi, H. Ma, Z.-K. Wang and L.-S. Liao, *Adv. Funct. Mater.*, 2015, **25**, 6671–6678.
138 J. Huang, S. Tan, P. D. Lund and H. Zhou, *Energy Environ. Sci.*, 2017, **10**, 2284–2311.
139 D. Angmo, X. Peng, A. Seeber, C. Zuo, M. Gao, Q. Hou, J. Yuan, Q. Zhang, Y. B. Cheng and D. Vak, *Small*, 2019, **15**, e1904422.
140 K. Zhang, Z. Wang, G. Wang, J. Wang, Y. Li, W. Qian, S. Zheng, S. Xiao and S. Yang, *Nat. Commun.*, 2020, **11**, 1006.
141 C. Duan, J. Cui, M. Zhang, Y. Han, S. Yang, H. Zhao, H. Bian, J. Yao, K. Zhao, Z. Liu and S. Liu, *Adv. Energy Mater.*, 2020, **10**, 2000691.

